FACULTY OF SCIENCE AND TECHNOLOGY

MASTER'S THESIS

Study program/specialization:
Marine and Offshore Technology

The spring semester, 2023
Open / ~~Confidential~~

Author:
Alejandro Garcia Conde

Supervisor:
Muk Chen Ong
Co-supervisor:
Xueliang Wen
Jianan Zhang

Thesis title:
Ballast Control Analysis of a Floating Dock under Accidental Conditions

Credits (ECTS): 30

Keywords:
PID control, Floating Dock, Dynamic Analysis,
Ballast Water Control, Critical Conditions,

Pages: 87
+ Appendix: 0

Stavanger, 14 June of 2023

Acknowledgments

I would like to thank Professor Muk Chen Ong, for being a mentor to all of his students from the Marine and Offshore Technologies master's program. His precise and valuable comments and our discussions have helped me to develop professionally and personally, and for this, he will always have my gratitude.

Among the resources offered to me by Professor Muk Chen Ong, the aid from Dr. Xueliang Wen and Jianan Zhang has been undoubtedly the most invaluable. If this work has been successful, it has been thanks to them, their patience and effort, and they deserve especial recognition.

Equally important support, the emotional, has come from my family. Even from the distance, they managed to encourage me and help me during the darkest days. Thank you.

Finally, I would like to extend my gratitude to all the professors and collaborators from the Marine and Offshore Technologies master's program for helping us become the professionals the industry needs, and to the Department of Mechanical and Structural Engineering and Materials Science for offering this degree and their resources involved in our learning.

Abstract

Floating docks play a critical role in the maintenance and inspection of submerged sections of ships. However, their operational complexity requires the expertise of a skilled dock master to develop an optimal ballast plan that minimizes heeling and trimming during operations. Unfortunately, recent years have witnessed several accidents involving floating docks, often attributable to component failures or human errors. To address these risks and proactively detect potential dock failures, an automatic controller for floating docks has been developed. The proposed modified P-controller serves as a valuable tool for facilitating both ballasting and de-ballasting operations while effectively maintaining the dock's roll and pitch angles close to zero, even when a vessel is docked on deck. To evaluate the controller's effectiveness, it is tested under various conditions, including scenarios where certain components of the ballast water system are non-functional. During the de-ballasting process, the dock successfully completes the operation. However, the closure of at least two tanks within the same circuit results in significant pitch angles, indicating a limitation of the controller under these conditions. Similarly, in the ballasting process without a docked vessel, the controller performs satisfactorily. However, when a vessel is present, the dock fails to achieve the desired draught of 10.1 m. These observations provide valuable insights into the potential benefits and limitations of the proposed automatic controller for floating docks. These findings underscore the importance of further research and development in this field to enhance the performance and capabilities of automatic controllers for floating docks. By addressing the limitations identified and refining the controller's functionality, the safety and efficiency of floating dock operations can be significantly improved.

Table of Contents

List of Figures

List of Tables

1. Introduction

1.1 Motivation and Background

As the regulations outlined in the International Convention for the Safety of Life at Sea (SOLAS) [1], vessels must undergo a dry docking inspection at least once every five years. This inspection is conducted to assess the condition of various submerged components of the vessel, including the hull, propeller, and rudder. Dry docks are facilities specifically designed to accommodate such inspections, and there are two primary types: graving dry docks, which are permanent structures situated along the coastline, and floating dry docks, which can be towed to the ship or relocated to different shipyards [2].

A floating dock is a floating marine structure in the form of a “U”, e.g., the one seen in Figure 1.1, where the bottom horizontal part is known as the pontoon, and the side vertical ones as wing walls. They are mainly used for salvaging operations, i.e., to rescue vessels involved in accidents that are unable to sail further to a coastal dock [3]. Nowadays, shipyards use these docks to handle smaller vessels rather than graving docks, which are often larger and more expensive. Floating docks offer more versatility, as different docks can be joined together to accommodate bigger ships.

Despite these benefits, there are drawbacks to floating docks. The chance of a floating dock sinking is one of the dangers involved. Floating docks are exposed to a variety of environmental conditions that can lead to damage and instability, such as severe winds, waves, and currents. Poor dock installation, design, or maintenance can worsen these problems and raise the risk of accidents. Overloading a dock over its weight limit occasionally causes structural failure and sinking.

Floating docks utilize the process of flooding or emptying the ballast water tanks installed within them to adjust their draught, following Archimedes' principle [4]. This adjustment in the total weight of the dock leads to a corresponding change in the dock's submerged volume. A hydraulic system, comprising tanks, pipes, pumps, and valves, facilitates the controlled inflow and outflow of water to and from the dock. Typically, this

operation is carried out by a skilled dock master who oversees the hydraulic system's operation. The dock master's responsibility is to maintain the dock's stability by carefully managing the hydraulic system to ensure minimal heel and trim angles are maintained, while also avoiding excessive stress due to deflection [5]. Given the dock master's expertise and extensive training, replacing such an experienced operator is a challenging task.

Figure 1.1. Floating dock during ship maintenance [3].

The primary objective of a regular procedure for a floating dock is to enable the inspection and maintenance of ships by lifting the vessel's keel above the water level, allowing for necessary interventions while ensuring the ship can be returned to a sailing condition. Throughout each stage of this process, specific operational limits must be taken into account as the stability of the floating dock varies with changes of the horizontal waterplane. Therefore, it is essential to differentiate and adhere to these limits to ensure a successful operation. The procedures of a normal de-ballasting operation are given in Figure 1.2 and shown as follows [6]:

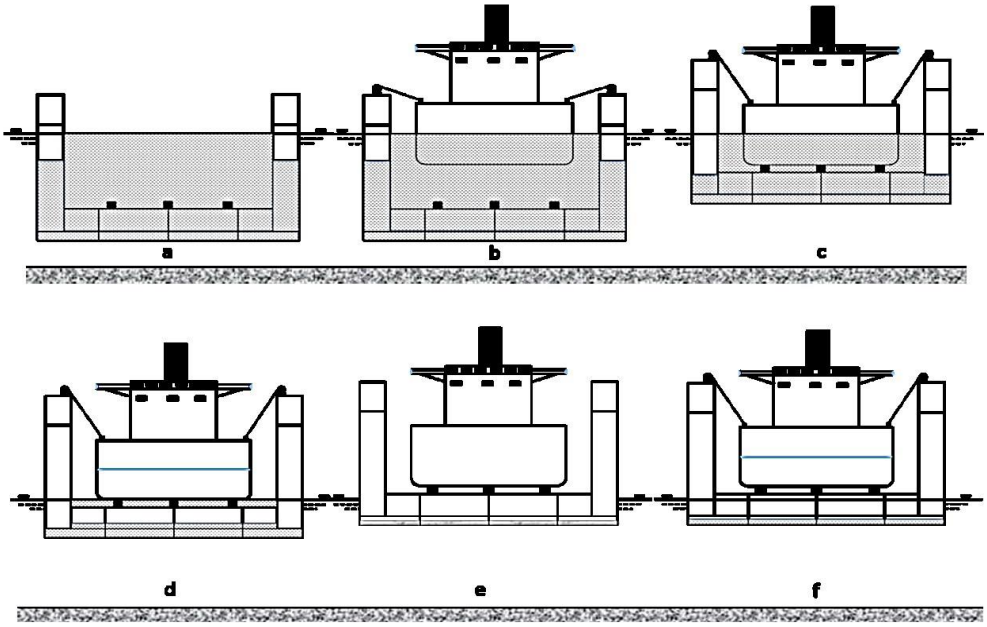

Figure 0.2. Emerging phases for a dock-vessel unit (a – dock immersion, b – docking, c – grounding a ship on keel blocks, d – keel blocks fully support the load, e – pontoon just below the water surface, f – dock emerged to the working position), reported by Rajewski [7].

(I) The dry dock pontoon is fully submerged, and the ship is not positioned yet. In this stage, the dock is lifted until the vertical distance between the ship's bottom and the top part of the keel blocks is at least 0.3 m. Then, the ship is positioned on top of the dock with the help of tugboats, following the positioning marks.

(II) The ship is partially lifted with docking blocks supported, approximately at half of its docking draught. The buoyancy force on the ship is reduced, and the weight of the ship is transferred into the dock.

(III) The external waterline reaches the top of the keel blocks. At this point, the whole ship is above sea level without any buoyancy. The area of waterplane of the entire floating dock system has a sudden decrease, which causes stability loss.

(IV) The waterline approaches the pontoon deck. The area of waterplane increases rapidly and the stability of the floating dock system increases.

(V) When the floating dock emerges to the planned working position, the de-ballasting process is stopped.

Developing an automatic controller for a floating dock to manage the ballast water system is important for several reasons:

- Operational Efficiency: An automatic controller can optimize the ballasting and de-ballasting processes. By automating these operations, the controller can precisely monitor and adjust ballast water levels, maintaining the dock's stability and trim within desired parameters. This reduces the need for manual intervention, saves time, and improves operational efficiency. It also minimizes the risk of human error, which can have safety implications.

- Cost Savings: Efficient management of the ballast water system can lead to cost savings. By automating the control and monitoring of ballast water, an automatic controller can optimize the system's performance, reducing energy consumption and operational costs. Additionally, timely detection of system malfunctions or failures through automated monitoring can help prevent costly repairs or damage to the dock or its equipment.

- Safety and Stability: A well-regulated ballast water system is crucial for maintaining the stability and safety of a floating dock. Uncontrolled ballasting or de-ballasting operations can affect the stability of the dock, posing risks to personnel, equipment, and cargo. An automatic controller can ensure that ballast water operations are carried out in a controlled manner, mitigating the potential risks associated with instability or improper weight distribution.

In summary, developing an automatic controller for the ballast water system of a floating dock is important to enhance operational efficiency, achieve cost savings, and ensure the safety and stability of the dock.

1.2 State of the Art

1.2.1 Automatic control of floating docks

Researchers have recently begun to look at floating docks' automatic ballast management. To address the issue, Ohkawa et al. (1984) [8] devised a control system that relies on maintaining the dock's movements within a permissible range. The model separated the dock's ballast tanks into several groups. The controller was fitted to the valve system to manage the trim, heel, and draught, allowing for the flooding or emptying of several sets of tanks. The low microcomputer processing power available at the time restricted them to utilize a straightforward linearized approach.

Guo et al. (2014) [9] discussed the hardware and software required for an autonomous floating dock in a more recent study. To determine the dock's heel and trim, they measured the deflection and draughts at each of its four corners and the center of the keel, at the port and starboard side. The heel and trim were kept within a permissible range by controlling the valve opening angles and the start or stop of the pump. Nevertheless, their study did not include any numerical results.

Similarly, Topalov et al. (2018) [10] created an algorithmic approach to regulate the heel and trim of the floating dry dock during the submerge and emerging operation based on physical input acquired from sensors. To keep track of the heel and trim angles, they employed a supervisory control and data acquisition (SCADA) system. To maintain the dock's stability, they created a strategy to distribute ballast in their research. Also, the dock's bending moment was measured and kept within acceptable limits.

Studies on the ballast control of various floating constructions are also available. Using a programmable logic controller (PLC), Kusuma (2017) [11] created a ballast control system for a catamaran ship. They displayed the procedure, the control plan, and the validation. Graph theory was used by Bara et al. (2012) [12] to develop a control approach for ship ballast systems that optimizes the ballasting process while consuming less energy.

A comprehensive numerical study of a floating dock system was developed by Zhang et al. [13]. They developed in-house software to model the motions of the dock and study

the ballast water distribution strategy. This model can fast predict the position of the dock during the ballasting or de-ballasting operations.

1.2.2 Accidents of floating docks and reported reasons

The utilization of the floating docks has an inherently higher risk than its ground counterpart due to the possibility of stability loss and capsizing. Accidents with floating docks are rare, but when they happen, the associated consequences are usually high [14]. Table 1.1 shows some examples of accidents related to floating docks in recent years. Many of the accidents can be attributed to problems in the ballast water system [2]. The ballast system is an essential component of a floating dock as it helps maintain the dock's stability by regulating the weight distribution. In some cases, the failure of one of the components of the ballast system can result in the loss of stability, which can cause the dock to capsize or sink.

The Dry Dock #3 accident took place in the Vigor Industrial Shipyard, Washington, in 2012. Due to a malfunctioning valve, the ballast water tank flooding caused additional listing that ended up in the sinking of the dock and the ship on top [15]. A different accident caused by the failure of the ballast tanks' valves occurred in Poland in 2015, at Remontowa Ship Repair Yard S.A. [16], where the ferry ship Prinsesse Benedikte slipped down from the keel blocks due to an excessive heeling of the dock, recorded in 13º, caused by a failure of the ballast tank's valve [7]. In the same location, in 2017, another floating dock located at Nauta Ship Repair, carrying the Norwegian tanker Hordafor V for repair, started to tilt and rested on its side due to human error [16].

The dock depends heavily on the ballast and de-ballast system to achieve the desired draught while maintaining the ship's structural integrity. Implementing an automatic control system for the ballast water system can minimize the risk of human error and decrease operating costs associated with training the dock's masters and workers. Additionally, it can establish operational boundaries and accident procedures. To mitigate accident casualties, it is crucial to conduct thorough testing of the dock's behavior and identify potential failure points that could lead to fatal accidents.

Table 1.1. Accidents related to floating docks in recent years.

Year	Dock's name	Shipyard	Location	Accident	Reason
2012	Dry Dock #3	Vigor Industrial Shipyard	USA	Excessive list angle caused the sinking of the dock and the ship on top	Malfunctioning valve
2015		Remontowa Ship Repair Yard	Poland	The ferry ship slipped down from the keel blocks	Failure in valve
2018	PD-50		Russia	The dock sunk, and one of the towers fell into the carried ship, causing a 5m hole	The ballast pump stopped working
2018	Floating dock No.169	Slavyanka Port	Russia	The starboard tower crane fell onto the deck due to an excessive list	Unclear, probably the wrong ballast plan added to improper maintenance
2018	SSR-1	Morska Stocznia Remontowa Gryfia	Poland	The dock developed a tilt and rested on its bottom	Failure in the ballast system
2019	PATO		Philippines	The FD sank during transport	Holes in the air vent system caused flooding of the tanks
2022	Tsakos	Montevideo Port	Uruguay	The dock listed, causing the cranes to slip and fall on the deck	Under investigation

Upon the investigation of some of these incidents, it was found that the ballast system's failure was often due to the malfunction of one of its components. When such accidents occur, dock masters often have to resort to various maneuvers to avoid fatal accidents. This can include modifying the ballast water plan, which can be challenging and unpredictable, especially in adverse weather conditions.

To reduce the risk of accidents involving the ballast system, a tool to monitor and control the ballast water system could be implemented. Such a tool could help maintain the stability and integrity of the dock while reducing the need for high-skilled workers and their associated costs. Furthermore, the implementation of such a tool could help reduce

fatal accidents and decrease the maintenance frequency of some components that may be redundant under the automatic controller's operation.

The dock depends heavily on the ballast and de-ballast system to achieve the desired draught while maintaining the ship's structural integrity. Overall, implementing a tool to monitor and control the ballast water system could significantly improve the safety and efficiency of floating docks, making them a more attractive option for shipyards and marinas. However, it is important to note that proper maintenance and inspections of the ballast system, as well as adherence to weight capacity limits and safety procedures, remain crucial in preventing accidents and ensuring the safety of those using the dock.

Accidents can happen even with the right maintenance program in place. Due to their long life expectancy and the high costs associated with new units, components of floating docks will fail during the life cycle of the dock. Establishing accident protocols and determining whether a component failure is important or not can be aided by understanding the effects that various failures can have on the dock and how they operate.

1.3 Objective

The present work aims to increase the safety and improve the efficiency of the floating dock by developing an automatic control system in a digital floating dock system, which can be served as a numerical model for the digital twin of the real floating dock. For this purpose, two industrial problems are intended to be solved:

1. How to automatically control the motions of the floating dock, by monitoring and distributing the ballast water in 18 tanks to reach the control targets.
2. Recognize irregularities in the ballast water system's components that might lead to an accident, and how to address the situation in case of an accident to optimize the operational time.

1.4 Scope of Work

In chapter 1 some background about floating dry docks is given, and the motivation for the present thesis is stated. A comprehensive overview of the existing literature and research related to the ballast water system of a floating dock is presented, with a brief review of some accident cases where floating docks were involved. The objectives of the work are defined, and a guide to the document is presented.

In chapter 2 the theoretical framework is defined.

In chapter 3 the methodology is explained. The numerical model and the setup used are described.

In chapter 4 an exhaustive numerical study of the automatic controller is presented.

In chapter 5 a dynamic analysis is performed when some components do not work as intended. Situations that can lead to an accident are evaluated, and the criticality of the components is assessed.

In chapter 6 the work performed in this thesis is collected in the conclusion, and the possibilities for future work are displayed.

2. Theory

2.1 Strip Theory

Solving a three-dimensional problem involving hydrodynamics and complex shapes can be challenging. A strip theory is a design methodology that is used in the design and analysis of engineering structures. It's a popular approach for analyzing the behavior of long, slender structures such as ships, bridges, pipelines, and tall buildings. Faltinsen and Svensen [18] performed an overview of seakeeping theories in 1990. They concluded that to determine the motions of a floating body, the most successful and practical tools are strip theories.

The basic idea of the theories is to divide the structure into a series of narrow strips or segments and analyze each strip individually. This allows engineers to simplify the analysis process, make it more manageable, and reduce the computational cost [19]. Each strip is modeled as a beam and its behavior is determined using beam theory. The behavior of the entire structure can then be obtained by combining the results from each strip. An example of the different strips composing a ship, taken from Bandyk [20], is shown in Figure 2.1.

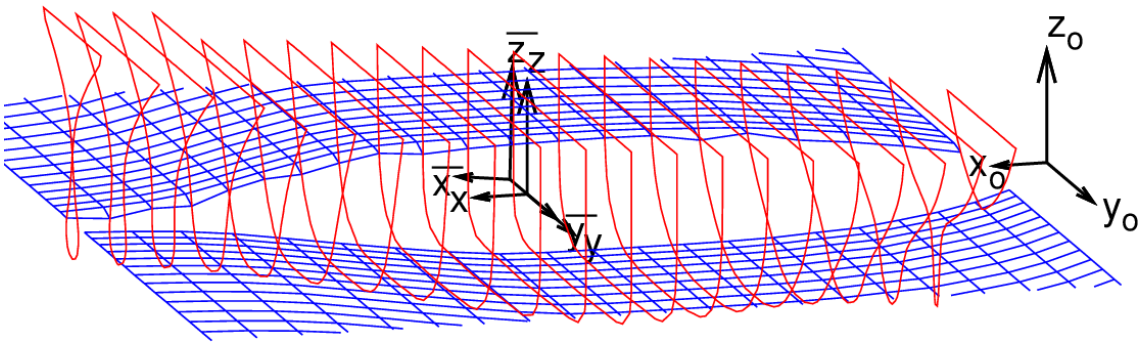

Figure 2.1. Discretization of a ship in several sections, using strip theory, reported from [20].

One of the restrictions of the theories is that only slender bodies are suitable for analysis. Faltinsen and the Seakeeping Committee of the 18th International Towing Tank Conference (ITTC) concluded that strip theories are effective for predicting ship motions with length-to-beam ratios as low as 2.5 [21]. Besides that, the strip theories are based on the potential flow theory. According to this, viscous effects are disregarded, which can cause serious issues when attempting to predict roll motions at resonance frequencies. Empirical methods can effectively account for viscous roll-damping effects in the real world.

Overall, strip theory is a useful design methodology that can be applied to a wide range of engineering structures, and is particularly well-suited for long, slender structures that are subject to bending and torsion.

2.2 PID Controller

Proportional-Integral-Derivative (PID) controllers are widely employed in control systems engineering and mechatronics. This control algorithm calculates an "error" value by comparing a desired setpoint (SP) with a measured process variable (PV). It then applies proportional, integral, and derivative terms to make corrections [22]. The primary objective of the PID controller is to minimize error by adjusting the control output.

A PID controller can be thought of as a combination of three separate controllers, each one with a specific function [23]. The proportional term applies a correction that is proportional to the error value. The integral term integrates the error over time and corrects systematic bias in the process. The derivative term provides a correction based on the rate of change of the error and helps to stabilize the system by anticipating future errors. The correction is calculated using Equation (2.1):

$$Correction = K_p(SP - PV) + K_i \int (SP - PV)dt + K_d \frac{d(SP - PV)}{dt} \quad (2.1)$$

where:

K_p is the proportional gain, a coefficient that adjusts the magnitude of the correction based on the error.

K_i is the integral gain, a coefficient that adjusts the magnitude of the correction based on the accumulated error over time.

K_d is the derivative gain, a coefficient that adjusts the magnitude of the correction based on the rate of change of the error.

SP is the set point, the desired value for the process variable.

PV is the process variable, the measured value of the process.

Tuning a PID controller is the process of adjusting the values of K_p, K_i, and K_d to achieve the desired performance in terms of stability, speed of response, and error minimization. There are various methods for tuning a PID controller, including trial and error, Ziegler-Nichols, and the Cohen-Coon method, among others [24].

PID controllers are widely used in a variety of applications, such as temperature control, motor control, process control, and robotics. However, they can sometimes exhibit undesirable behavior, such as overshoot, oscillation, or slow response, if the gains are not set correctly.

3. Methodology

3.1 Model setup

The floating dock under investigation is shown in Figure 3.1. The design of the floating dock is based on realistic data commonly used for such structures. The behavior of the dock changes when there is a docked ship on top. The ship geometry presented in Figure 3.2, is added to the model to assess the differences during operation, with and without the ship. The dimensions of the floating dock, length (L), breadth (B), and height (H), along with the mass moments of inertia and the dry mass, are provided in Table 3.1.

Inside the dock, there are a total of eighteen ballast tanks, arranged in a 3×6 array, as presented in Figure 3.3. Hydraulic pumps are located at the port side of the dock, as seen in Figure 3.4. Each pump can de-ballast the water in three tanks from the port side to the starboard side, and at the same time, the inlet and outlet circuits share the same pipes, except for the ones connected to the outside. While the de-ballasting process is done with hydraulic pumps, the gravitational ballasting process is conducted by opening the valves connected to the open sea and letting water flow in due to pressure differences.

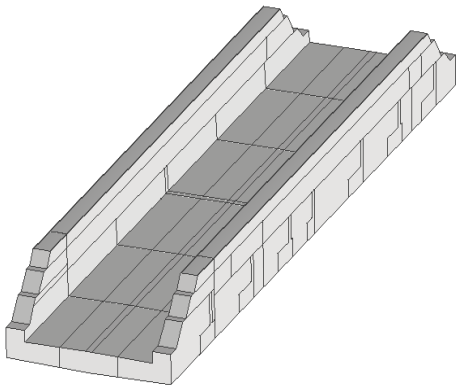

Figure 3.1. Floating dock model geometry.

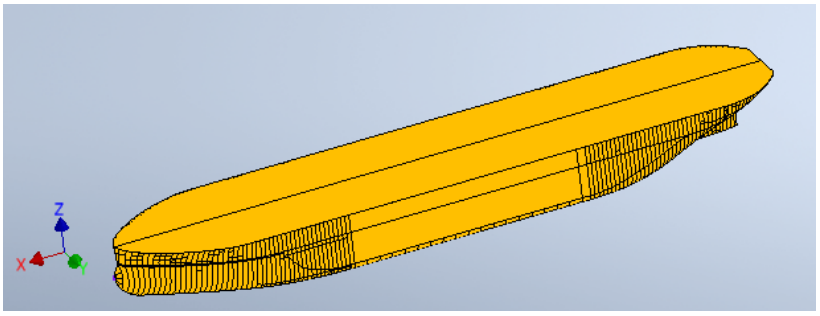

Figure 3.2. The geometry of the ship docked on the floating dock.

Table 3.1. Model dimensions, mass moments of inertia, and dry mass.

	Dock	Ship
L (m)	168.48	91.59
B (m)	39.8	20
H (m)	18.34	8.53
I_{xx} (kg·m^2)	1.18×10^{9}	2.23×10^{8}
I_{yy} (kg·m^2)	1.09×10^{10}	2.97×10^{9}
I_{zz} (kg·m^2)	1.18×10^{10}	2.97×10^{9}
Mass (ton)	4530	5129

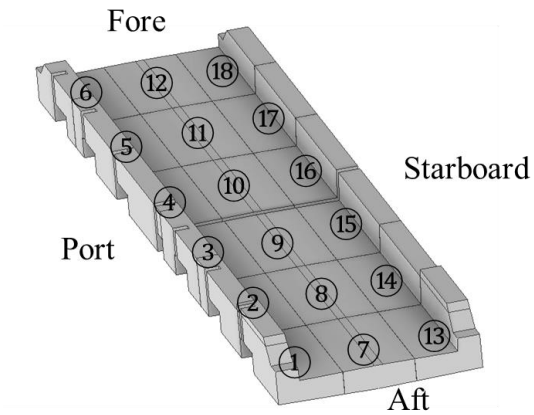

Figure 3.3. Ballast tanks geometry and position in the floating dock

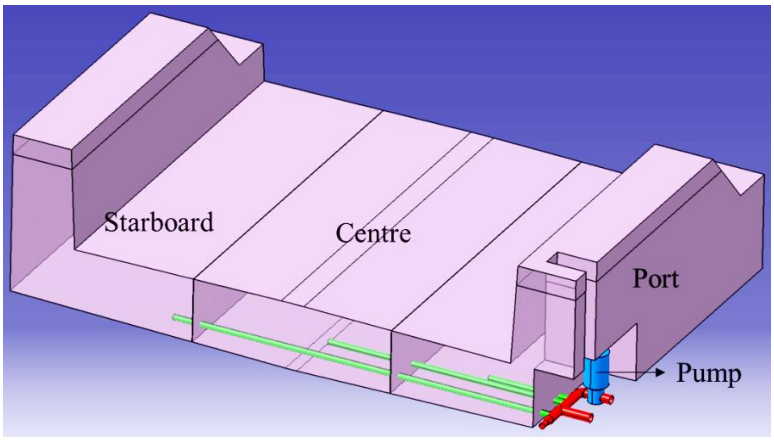

Figure 3.4. Detail of one of the hydraulic systems

3.2 Controller Setup

The primary objective of the controller is to enable the adjustment of the floating dock's draught to meet the specific operational requirements while maintaining the stability of both the dock and the docked ship. The draught of the dock is controlled by managing the ballast water stored within its tanks, allowing for controlled inflow or outflow of water. To achieve this, the controller incorporates three distinct groups of components:

- The de-ballasting pumps will be turned on during the de-ballast operation and turned off during the ballast operation.
- The inlet valves, that are opened during the ballasting operation to allow the flow of water into the ballast tanks.
- The butterfly valves located inside the ballast system pipes, or ballast tanks' valves, regulate the flow going into each ballast tank.

The controller primarily focuses on the valves of the ballast tanks, with its responsibility being the management of the opening and closing of these valves. This control mechanism regulates the inflow of water into each tank during the ballasting process and the outflow of water during de-ballasting operations. The valves in the middle are fully opened. The present controller sets the target angle for the valves located in the port and starboard. The valves of side tanks are divided into four groups: fore-port, fore-

starboard, aft-port, and aft-starboard. The target angle ($\theta_{i,target}$) of each control group is calculated with Equation (3.1) in the present controller.

$$\theta_{i,target} = \theta_{max}\min\{1 + K_p c_{i,p} L\psi + K_r c_{i,r} B\gamma, 1\} \tag{3.1}$$

where the control group, pitch, and roll control coefficients for the ballasting operation are listed in Table 3.2. The proportional gain for pitch (K_p) and roll (K_r) motion are defined as a function of the water plane area of the dock.

Table 3.2. Control group, pitch, and roll control coefficients for the ballasting operation.

	Fore-port	Fore-starboard	Aft-port	Aft-starboard
Tank No.	4, 5, 6	16, 17, 18	1, 2, 3	13, 14, 15
$c_{i,p}$	1	1	-1	-1
$c_{i,r}$	-1	1	-1	1

In every time step, the pitch and roll angles are evaluated, and the controller acts accordingly in each valve group when these values exceed the defined limit. Equation (3.1) only provides a control signal, the real valve opening angle is affected by the valve angular speed.

Note that the current controller exclusively utilizes the proportional control component. The integral and derivative terms are not incorporated into the controller due to the quasi-static nature of the dock's movements. As the set point is not directly proportional to the required correction, this type of controller can be categorized as a modified proportional controller.

3.3 Hydrostatic Model

The stability of a floating object relies on the equilibrium between two forces: gravitational force and buoyant force. In the case of a floating dock, the gravitational force is determined by its total mass (m) and varies as the ballast water content changes. Conversely, the buoyant force is dependent on the submerged volume (∇) of the dock. According to Archimedes' principle, the buoyant force required to maintain stability increases as the weight on the dock rises, as in Equation (3.2). For all the calculations, the gravitational acceleration (g) is set at 9.81 m/s^2, while the water density (ρ_w) is 1025 kg/m^3.

Hydrostatic forces acting on the dock are computed using a strip theory. The dock, its ballast tanks, and the docked ship are divided into sections along the longitudinal direction. Figure 3.5 illustrates the strip discretization, showcasing the distinct sections that have been created for the floating dock. The hydrostatic forces of the entire body are obtained by integrating the individual results from the sections.

Thus, the weight of the dock W is obtained by Archimedes' principle, as per Equation (3.3), and subsequently, the heeling M_{heel} and trimming M_{trim} moments, as per Equations (3.4) and (3.5), where ρ is the density of water, A_{sub} is the cross-sectional area under water, and x_{CG} and y_{CG} are the x- and y-coordinates of the center of gravity of the dock. The hydrostatics forces for each of the ballast tanks are determined and added up to the total dock forces.

$$mg = \rho_w g \nabla \tag{3.2}$$

$$W = \rho_w \int A_{sub} dx \tag{3.3}$$

$$M_{heel} = \rho_w \int A_{sub} \, (y - y_{CG}) \, dx \tag{3.4}$$

$$M_{trim} = -\rho_w \int A_{sub} \, (x - x_{CG}) \, dx \tag{3.5}$$

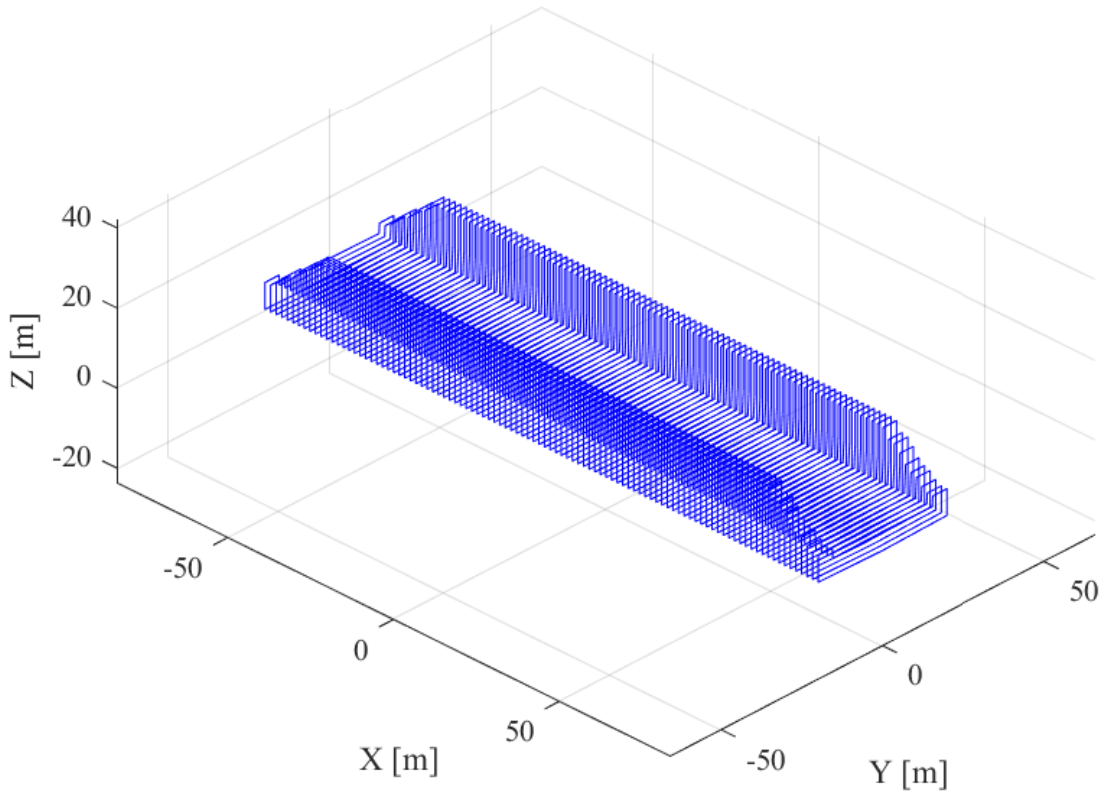

Figure 3.5. Floating dock discretization in strips along the longitudinal axis.

3.4 Hydrodynamic Model

Hydrodynamic forces are the forces exerted by a fluid on a submerged body or when it moves through the fluid. These forces are influenced by various factors such as the viscosity of the fluid, pressure distribution, and the relative velocity between the body and the fluid. Understanding and accurately predicting these forces are of utmost importance as they significantly affect the performance, stability, and safety of structures operating in fluid environments.

When analyzing the dynamic response of a floating dock, it is essential to consider the damping coefficient of the structure. In this regard, modeling and refinement of the damping coefficients have been conducted using an approximate model of the current floating dock. The calculation of these coefficients incorporates the natural frequencies associated with the heave, roll, and pitch motions of both the dock and the ship. The mass

matrix is also taken into account, along with a damping ratio of 5%. This comprehensive approach aids in accurately determining the dynamic behavior of the floating dock.

In addition, it is crucial to consider the added mass effect exerted on the floating dock by the surrounding fluid. The added mass phenomenon occurs when an object moves through a fluid, resulting in an increase in its effective mass due to the presence of the fluid [25, 26]. As the object moves, the fluid resists its motion and flows around it, creating a force that leads to the concept of added mass. This force causes the object to behave as if it has a greater mass than its physical mass alone. To determine the added mass and the added mass moment of inertia, the strip theory is employed. This involves integrating the individual results obtained for a 2D plate in each strip along the length of the dock. By applying this methodology, the added mass and added mass moment of inertia can be accurately calculated for the floating dock, considering the influence of the surrounding fluid.

3.5 Hydraulic Model

The hydraulic system of the floating dock primarily serves the purpose of ballasting and de-ballasting the water within the ballast tanks. This system consists of six hydraulic units, with each unit comprising three ballast tanks: one located in the center, one on the port side, and one on the starboard side, as shown in Figure 3.6. These ballast tanks connect to the main pipe through a 400 mm pipe. To regulate the flow of water in these three pipes, each pipe is equipped with a butterfly valve. The main pipe, with a diameter of 600 mm, acts as a conduit, linking the ballast tank pipes to the inlet and outlet pipes of the hydraulic system. This arrangement allows for effective control of water flow during the ballasting and de-ballasting operations of the floating dock.

To ensure safety in the design, the opposite end of the main pipe is connected to a pipe that interconnects the other five hydraulic units. This pipe is equipped with a butterfly valve, which is typically kept closed. The purpose of this arrangement is to provide a safety measure when one of the six pumps fails. The inlet pipe, which allows water to enter the ballast tanks, is regulated by another butterfly valve. This pipe is connected to the exterior,

and when the inlet valve is opened, water enters the ballast tanks through the force of gravity, without requiring any external energy. However, to drain or empty the ballast tanks, external energy is needed. For this purpose, an outlet pipe is installed with a centrifugal pump that increases the pressure within the hydraulic circuit. Additionally, a control valve is incorporated into the outlet pipe to regulate the flow rate after the pump. This setup enables the efficient removal of water from the ballast tanks when required.

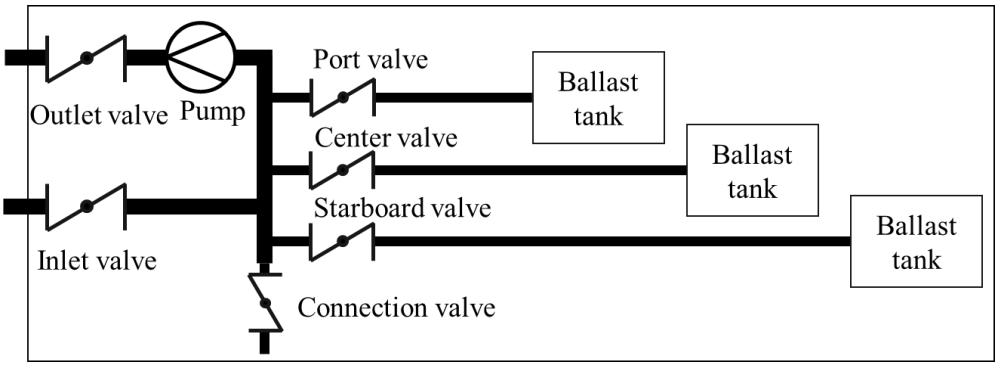

Figure 3.6. Hydraulic unit of the floating dock ballast system.

The pressure variations of various elements, such as the pipes, valves, and pumps, form the foundation for the hydraulic calculations of the ballast water system. The pressure variations brought on by valves and pumps are taken into account, but pressure loss caused by the friction head along the pipes is disregarded because of the short length of the pipes. Equations (3.6) – (3.9) are used to compute the water head at the outlet, port, center, and starboard valves.

$$h_{\mathrm{O}} - h_{\mathrm{out}} = \lambda_{\mathrm{M}} |Q_{\mathrm{M}}| Q_{\mathrm{M}} \tag{3.6}$$

$$h_{\mathrm{P}} - h_{\mathrm{M}} = \lambda_{P} |Q_{\mathrm{P}}| Q_{\mathrm{P}} \tag{3.7}$$

$$h_{\mathrm{C}} - h_{\mathrm{M}} = \lambda_{\mathrm{C}} |Q_{\mathrm{C}}| Q_{\mathrm{C}} \tag{3.8}$$

$$h_{\mathrm{S}} - h_{\mathrm{M}} = \lambda_{\mathrm{S}} |Q_{\mathrm{S}}| Q_{\mathrm{S}} \tag{3.9}$$

The valve coefficients, denoted as λ, are determined using Equation (3.10), which involves the utilization of the K_V value, a convenient value for valve size selection. The K_V value, also known as the flow coefficient, represents the flow rate in m^3 of a fluid with a specific gravity of one, at a pressure drop of one bar. This value is typically provided by the valve manufacturer [27] and serves as an essential parameter in the calculation of the valve coefficients. The K_V values for both types of valves are shown in Figure 3.7. The pump shut-off head h_0 is 21.75 m, determined with Equation (3.11), when the net flow in the main pipe Q_M is null, where the pump coefficient λ_{pump} is 20 s^2/m^5.

$$\lambda = \frac{1}{g\left(\frac{K_V}{36000}\right)^2} \tag{3.10}$$

$$h_0 = h_O - h_M + \lambda_{pump}|Q_M|Q_M \tag{3.11}$$

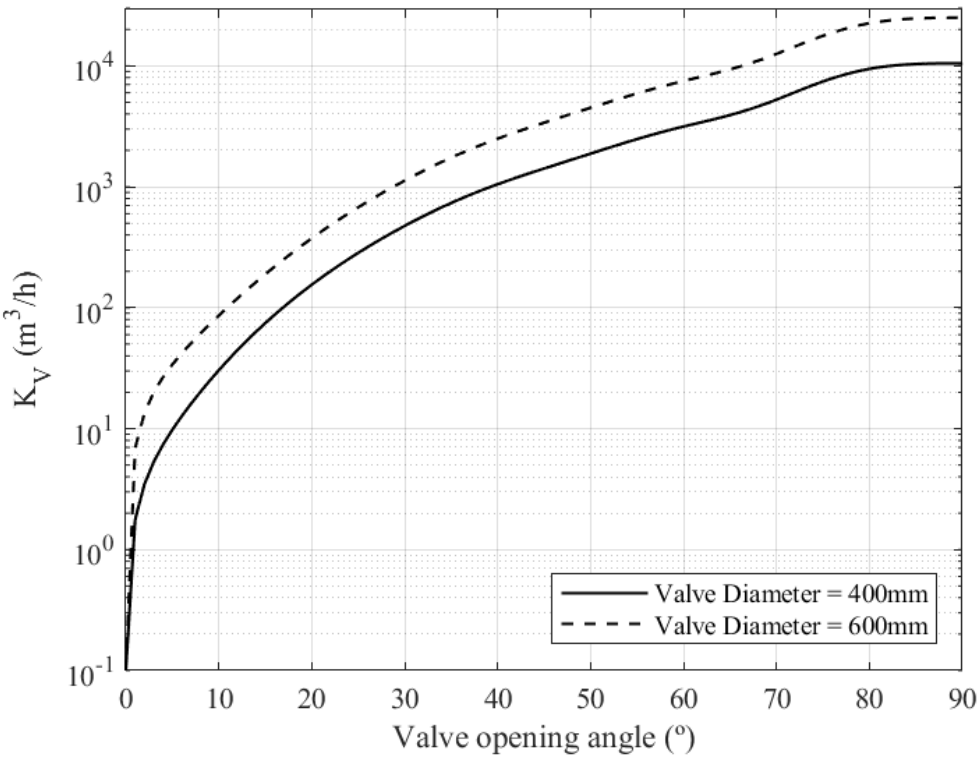

Figure 3.7. K_V parameters for the different valve types at different opening angles.

From Equations (3.7) – (3.9) an expression for the flow in each pipe is obtained, and the Ω parameters defined as shown in Equations (3.12) – (3.15). Subtracting Equation (3.6) to (3.11), an expression for the flow in the main pipe Q_M is obtained, in Equation (3.15).

$$Q_P = \sqrt{\frac{1}{\lambda_P(h_P - h_M)}}(h_P - h_M) = \Omega_P(h_P - h_M) \tag{3.12}$$

$$Q_C = \sqrt{\frac{1}{\lambda_C(h_C - h_M)}}(h_C - h_M) = \Omega_C(h_C - h_M) \tag{3.13}$$

$$Q_S = \sqrt{\frac{1}{\lambda_S(h_S - h_M)}}(h_S - h_M) = \Omega_S(h_S - h_M) \tag{3.14}$$

$$\begin{aligned} Q_M &= \sqrt{\frac{1}{(\lambda_{pump} + \lambda_M)(h_0 - h_{out} + h_M)}}(h_0 - h_{out} + h_M) \\ &= \Omega_M(h_0 - h_{out} + h_M) \end{aligned} \tag{3.15}$$

Following the continuity equation, the total flow in the main pipe Q_M should be equal to the summation of the port, center, and starboard pipes flow, thus Equation (3.16) is obtained. By substituting Equations (3.12) – (3.15) into (3.16), the head in the main pipe h_M is obtained, as per Equation (3.17), where the different Ω are iteration coefficients. Note that the valve coefficients are functions of h_M, therefore an iterative solver is used to approximate the solution.

$$Q_M = Q_P + Q_C + Q_S \tag{3.16}$$

$$h_M = \frac{\Omega_P h_P + \Omega_C h_C + \Omega_S h_S + \Omega_M(h_{out} - h_0)}{\Omega_P + \Omega_C + \Omega_S + \Omega_M} \tag{3.17}$$

In every time step, the net flow in each valve is determined using the convergence value of the main pipe head, and the ballast tank volume fraction of water is updated accordingly. For the next time step, the head in each of the valves changes due to the difference in water height inside the tanks. Thus, the flow distribution variates at every time step.

In the de-ballasting operation, the pump is turned on and the outlet valve is fully open, while the inlet valve is closed. On the contrary, in the ballasting operation, the inlet valve is open and the outlet valve is closed, and the pump is turned off (the pump shut-off head and the pump coefficient are set to zero). The pressure difference between the ballast tanks and the inlet valve allows the ballast water to come down by gravity forces.

3.6 Six Degrees of Freedom Model

The floating dock is modeled as a rigid body with six degrees of freedom (6-DOF), and thus rigid body kinematics are applied to determine the three translational degrees of freedom (surge, sway, and heave) and the three rotational degrees of freedom (roll γ, pitch ψ, and yaw ϕ), as described in Figure 3.8. Newton's second law is used to obtain the translational motions in the global reference frame as Equation (3.18):

$$\boldsymbol{m}\frac{d^2\hat{r}_{CG}}{dt^2} = \sum \hat{F}_G \tag{3.18}$$

where $\boldsymbol{m}$ is the mass matrix, $\hat{r}_{CG}$ is the position vector in the global reference frame, and $\hat{F}_G$ the external forces, obtained as the sum between the buoyant force and the weight. The buoyancy force Δ is obtained using Arquimedes' principle, where the buoyant force is equal to the weight of water displaced by the submerged volume of the floating body ∇, as in Equation (3.19). To determine the angular motions in the local reference system, Euler's rotation Equation (3.20) is solved to obtain the angular accelerations [28].

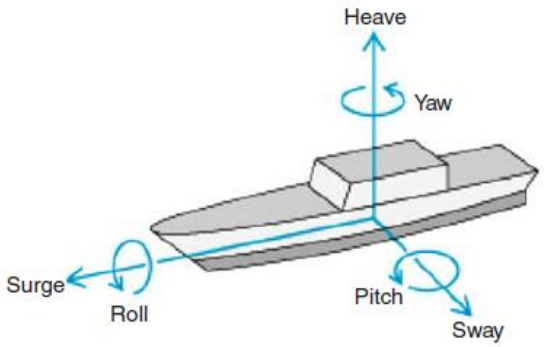

Figure 3.8. 6-DOF used for the ship and the floating dock, reproduced from [4].

$$\Delta = \rho g \nabla \tag{3.19}$$

$$\boldsymbol{I}\hat{\dot{\omega}} + \hat{\omega} \times (\boldsymbol{I}\hat{\omega}) = \hat{M} \tag{3.20}$$

where $\boldsymbol{I}$ is the inertial tensor, $\hat{\dot{\omega}}$ the angular acceleration, $\hat{\omega} = (\omega_1, \omega_2, \omega_3)$ the angular velocity, and $\hat{M}$ the torque applied in the center of gravity. The torque is calculated by integrating the external loads over the dock's dimensions. The angular speed of the rotational degrees of freedom in the global reference frame is obtained by applying the kinematic differential Equation (3.21):

$$\begin{pmatrix} \dot{\phi} \\ \dot{\psi} \\ \dot{\gamma} \end{pmatrix} = \frac{1}{\cos\theta} \begin{bmatrix} 0 & \sin\gamma & \cos\gamma \\ 0 & \cos\gamma\cos\psi & -\sin\gamma\cos\psi \\ \cos\psi & \sin\gamma\cos\psi & \cos\gamma\sin\psi \end{bmatrix} \begin{pmatrix} \omega_1 \\ \omega_2 \\ \omega_3 \end{pmatrix} \tag{3.21}$$

In the present 6-DOF model, the interaction between the dock and the vessel is addressed approximately. Before the vessel contacts the blocks on the pontoon deck, the dock's motions are updated based on its mass, mass moments of inertia, and the external forces acting on the dock. After the vessel touches the blocks, the dock and the vessel are considered as a single rigid body with hybrid mass and mass moments of inertia.

4. Numerical Study on the Automatic Ballast Control of a Floating Dock*

Abstract

The ballast control of a floating dock mainly relies on manual operations, which can be time-consuming and requires skilled workers. This study proposes an automatic ballast control system for floating docks, which improves operational efficiency and safety during the vessel docking process. A numerical model is developed to simulate the dynamic process of the floating dock's operations, which includes a six-degree-of-freedom (6-DOF) model, a hydrostatic force model, a hydrodynamic force model, and a hydraulic model. The proposed automatic ballast control system is based on a modified P-controller, which controls the valve opening angles when the pitch or roll angles exceed specific threshold values. The hydrostatic force model is developed using Archimedes' law and a strip theory along the longitudinal direction. The hydrodynamic model is made based on the effects of added mass and dynamic damping. The hydraulic model is proposed to deal with the hydraulic calculation of the ballast water system. The present automatic ballast control is designed based on a proportional controller to control the valve opening angles when the pitch or roll angles are larger than the corresponding threshold values. Results show that the roll angles of the dock can reach 8.9deg and 13deg for the ballasting and de-ballasting operations without controllers, respectively. The present modified P-controller with optimized control parameters can stabilize the dock and keep the maximum pitch and roll angles no larger than 0.016deg and 0.0783deg, respectively. The present automatic control will be further implemented in the vessel docking cases and can significantly improve the stability of the dock.

* The content of this chapter is submitted to Journal OMAE for publication

4.1 Introduction

A complete survey should be carried out regularly on dry docks in the lifetime of a ship, including the maintenance of the hull, propeller, rudder, and other parts immersed in seawater. There are mainly two types of dry docks [3], i.e., graving docks and floating docks. Nowadays, floating dry docks installed in sheltered harbors near the shore are commonly used for the maintenance of sea-going vessels.

A floating dock includes a pontoon deck, two wing walls, and multi-ballast tanks under the deck and inside the wing walls. The main docking stages of a typical ship docking operation [29] are shown in Figure 4.1. The stages are listed as:

(a) A floating dock equipped with docking blocks is submerged to a specified draught required in the docking plan.

(b) A vessel is positioned above the docking blocks with the help of tugboats and then tied to the dock.

(c) De-ballasting starts and the ballast water is pumped out. The floating dock is lifted until the vessel's stern touches the docking blocks.

(d) The de-ballasting continues until the vessel is fully loaded on the blocks.

(e) When the floating dock emerges to the planned working position, the pumping process is stopped.

The ballast control operation is crucial for maintaining the stability of a floating dock during the docking process. Currently, ballast control is mainly performed manually by skilled workers, who must handle numerous ballast tanks and valves to keep the dock stable while a vessel docks. However, this task is challenging, and even minor mistakes can result in significant stability loss for both the dock and the docked vessel. To improve the accuracy and efficiency of ballast water adjustments, an automatic ballast control system is necessary. Additionally, implementing this system on a floating dock can reduce the number of required staff and associated training costs for the shipyard. Therefore, studying and implementing an automatic ballast control system has the potential to enhance safety, efficiency, and cost-effectiveness in the docking process.

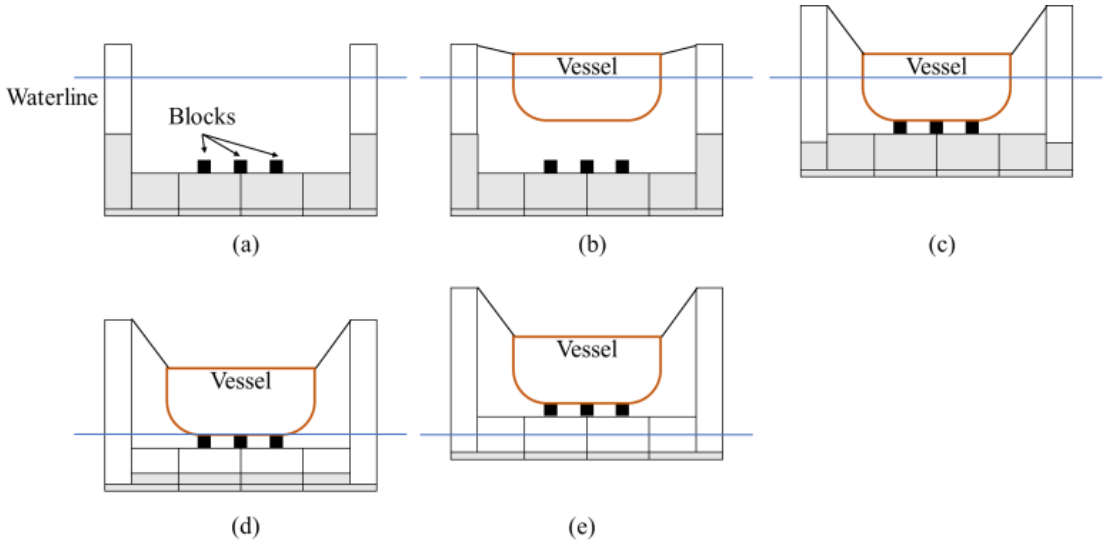

Figure 4.1. Different docking stages of a floating dock during the de-ballasting operations [29].

In recent decades, researchers have started to study the automatic ballast control of floating docks based on experimental measurements. Ohkawa et al. [8] developed a simple linearized algorithm to keep the dock's draught, heel, and trim within allowable ranges. The dock's ballast tanks were divided into several groups to control the draught, heel, and trim independently. The controllers were applied to the ballast valves, enabling the filling or emptying of different groups of tanks. Guo et al. [9] described the hardware and software necessary for an automatic ballast control of a floating dock. They monitored the draughts at six locations on the dock to calculate the dock's heel and trim. The valve opening angles and the start or stop of the pumps were controlled to keep the heel and trim angles within allowable ranges. Topalov et al. [10] developed an algorithm based on physical input obtained from sensors to control the heel and trim angles of the floating dock during the submerging and emerging operations. They used the supervisory control and data acquisition (SCADA) system to monitor the heel and trim angles. Their study produced the ballast water adjustment plan to keep the dock stable. Moreover, the bending moment of the dock was monitored and kept below a threshold value. These studies on the automatic ballast control of the floating docks are based on experiments. However, the experiments are expensive and time-consuming. Numerical simulations on the floating docks with automatic ballast control

should be performed before conducting the experiments on the real docks, which will significantly reduce the experimental cost and human errors.

There are also studies on the ballast control of other floating structures. Kusuma [11] designed a ballast control system for a catamaran ship using a programmable logic controller (PLC) to increase the stability of the catamaran-type ship. Bara et al. [12] developed a control strategy for the ship ballasting system to optimize the ballasting procedures and reduce energy consumption. Therefore, the development of automatic ballast control based on a numerical method can benefit different types of floating structures.

In the present study, the automatic ballast control is studied using a numerical model developed for simulating the dynamic process of a floating dock during docking operations. The automatic ballast control should ensure a stable dock with small allowable ranges of heel and trim angles. The present work is organized as follows. First, the numerical model of a floating dock including a six-degree-of-freedom (6-DOF) model, a hydrostatic force model, a hydrodynamic force model, and a hydraulic model is presented. Then, the present automatic ballast control strategy is proposed based on the classical proportional controller. Finally, the time-domain simulations of the floating dock with and without the present automatic ballast control strategy are performed using the developed numerical model. By presenting the numerical model and the results of the simulations, this study provides insights into the potential benefits of implementing an automatic ballast control system for enhancing the stability and safety of floating docks during docking operations.

4.2 Methodology

4.2.1 Description of a floating dock system

Figure 4.2 shows the floating dock system, which consists of a floating dock, a vessel, mooring ropes connecting the dock and the vessel, mooring lines attached to the dock, and docking blocks on the pontoon deck. The specifications of the floating dock system are summarized in Table 4.1. The dock's center of gravity (CoG) in a global coordinate system *OXYZ* is provided, with the origin at the keel's center. The *X*-axis is along the longitudinal

direction from aft to fore, the Y-axis from starboard to port, and the *Z*-axis vertically upward from the bottom of the dock. Initially, a body-fixed coordinate system *oxyz* is identical to the global coordinate system but changes as the dock moves.

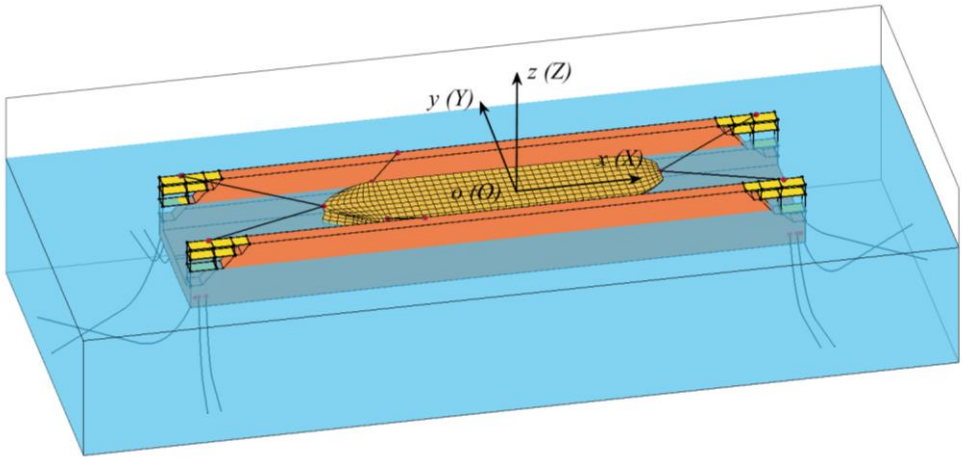

Figure 4.2. Schematic of a floating dock system.

Table 4.1. Floating dock specifications.

Dimension of dock $L \times B \times H$	$168.48\text{m} \times 39.8\text{m} \times 18.2\text{m}$
Mass of dock (including blocks)	$5.1782 \times 10^6\text{kg}$
Initial CoG of the dock	$(-0.435\text{m}, 0.093\text{m}, 5.497\text{m})$
Inertia of dock $I_{11\text{dock}}$	$9.55 \times 10^8\text{kg} \cdot \text{m}^2$
Inertia of dock $I_{22\text{dock}}$	$1.026 \times 10^{10}\ \text{kg} \cdot \text{m}^2$
Inertia of dock $I_{33\text{dock}}$	$1.096 \times 10^{10}\ \text{kg} \cdot \text{m}^2$
Density of seawater	1025kg/m^3
Gravitational acceleration	9.81m/s^2

Figure 4.3 shows 18 ballast tanks equipped inside the floating dock. Their geometries are different between the port and starboard sides, e.g., Tank No.01 and Tank No.13, and between the bow and stern, e.g., Tank No.01 and Tank No.06. Thus, the distribution of the

ballast tanks is asymmetric inside the floating dock. Additionally, there are six ballast pumps installed on the port side of the dock. Table 4.2 provides the maximum volumes V_{max} of the 18 tanks.

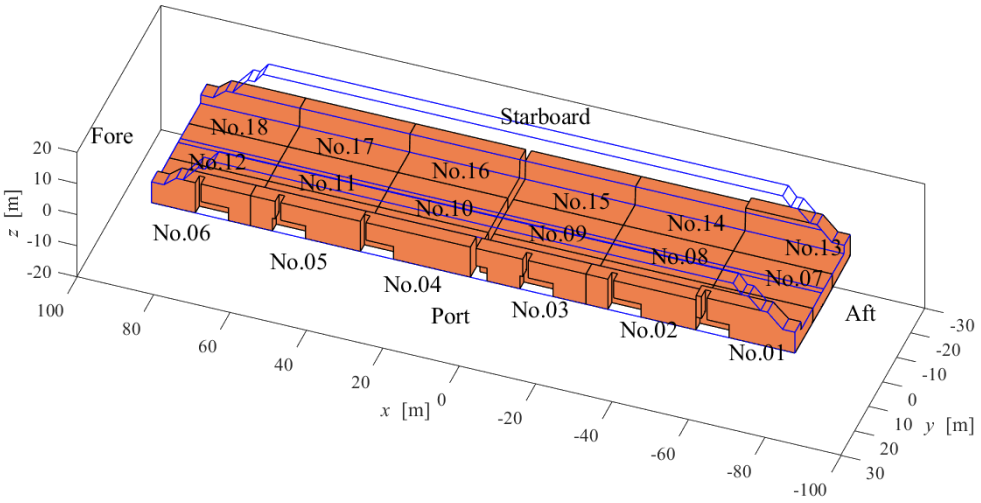

Figure 4.3. Description and numbering of the ballast tanks.

Table 4.2. V_{max} of different ballast tanks.

No.	1	2	3	4-5	6	7,12	8-11	13	14-17	18
$V_{\max}$ [m^3]	1965	2144	2110	2145	1856	1653	1837	2093	2067	1978

4.2.2 6-DOF model

The 6-DOF model is utilized to calculate the motions of the floating dock and the docked vessel. The governing equation of the dock or vessel's translational motions in the global coordinate system is presented in Equation (4.1) which is derived from Newton's Second Law.

$$\frac{\mathrm{d}^2 \boldsymbol{X}_{CG}}{\mathrm{d}t^2} = \boldsymbol{m}^{-1} \sum \boldsymbol{F}_G \tag{4.1}$$

where $\boldsymbol{X}_{CG} = (X_{\mathrm{CG}}, Y_{\mathrm{CG}}, Z_{\mathrm{CG}})$ is the location of the CoG, and $\boldsymbol{m}$ is the mass matrix of the dock or the vessel. $\boldsymbol{F}_{\mathrm{G}}$ is the vector of external forces applied to the CoG. The dock's or the vessel's angular velocity vector in the body-fixed coordinate system is calculated using Equation (4.2) [28].

$$\frac{\mathrm{d}\boldsymbol{\omega}_{\mathrm{B}}}{\mathrm{d}t} = \boldsymbol{I}^{-1}\left[\sum \boldsymbol{M}_{\mathrm{B}} - \boldsymbol{\omega}_{\mathrm{B}} \times (\boldsymbol{I}\boldsymbol{\omega}_{\mathrm{B}})\right] \tag{4.2}$$

where $\boldsymbol{I}$ is the inertial tensor, $\boldsymbol{M}_{\mathrm{B}}$ is the moment vector acting on the dock's or the vessel's CoG and $\boldsymbol{\omega}_{\mathrm{B}} = (\omega_{B1}, \omega_{B2}, \omega_{B3})$ is the dock's or the vessel's angular velocity vector. The subscript "B" means that the variables are in the body-fixed coordinate system. The rotational angles of the rigid body are computed using Equation (4.3) [28].

$$\begin{cases} \dfrac{\mathrm{d}\phi}{\mathrm{d}t} = (\omega_{B2}\sin\gamma + \omega_{B3}\cos\gamma)/\cos\psi \\ \dfrac{\mathrm{d}\psi}{\mathrm{d}t} = (\omega_{B2}\cos\gamma - \omega_{B3}\sin\gamma) \\ \dfrac{\mathrm{d}\gamma}{\mathrm{d}t} = \omega_{B1} + (\omega_{B2}\sin\gamma + \omega_{B3}\cos\gamma)\tan\psi \end{cases} \tag{4.3}$$

where ϕ, ψ, and γ are the yaw, pitch, and roll angles, respectively. The position of a point on the dock or vessel in the global coordinate system can be obtained from its position in the body-fixed coordinate systems using Equation (4.4) based on the coordinate transformations of rotation axes.

$$\begin{bmatrix} X - X_{CG} \\ Y - Y_{CG} \\ Z - Z_{CG} \end{bmatrix} = R_\phi R_\psi R_\gamma \begin{bmatrix} x - x_{CG} \\ y - y_{CG} \\ z - z_{CG} \end{bmatrix} \tag{4.4}$$

where

$$R_\phi = \begin{bmatrix} \cos\phi & -\sin\phi & 0 \\ \sin\phi & \cos\phi & 0 \\ 0 & 0 & 1 \end{bmatrix} \tag{4.5}$$

$$R_\psi = \begin{bmatrix} \cos\psi & 0 & \sin\psi \\ 0 & 1 & 0 \\ -\sin\psi & 0 & \cos\psi \end{bmatrix} \tag{4.6}$$

$$R_\gamma = \begin{bmatrix} 1 & 0 & 0 \\ 0 & \cos\gamma & -\sin\gamma \\ 0 & \sin\gamma & \cos\gamma \end{bmatrix} \tag{4.7}$$

4.2.3 Hydrostatic force model

The hydrostatic forces, which include the buoyancy forces acting on the dock and vessel and the gravitational forces due to water in the ballast tanks, are calculated using Archimedes' principle. A strip theory is adopted to calculate the volume of the immersed part of the dock (or vessel) and the volume of water in the ballast tanks. The three-dimensional (3D) body of the dock and the ballast tanks are sliced into two-dimensional (2D) sections and shown in Figure 4.4 and Figure 4.5, respectively, where 30 sections of the dock and 20 sections of the tanks are depicted as examples.

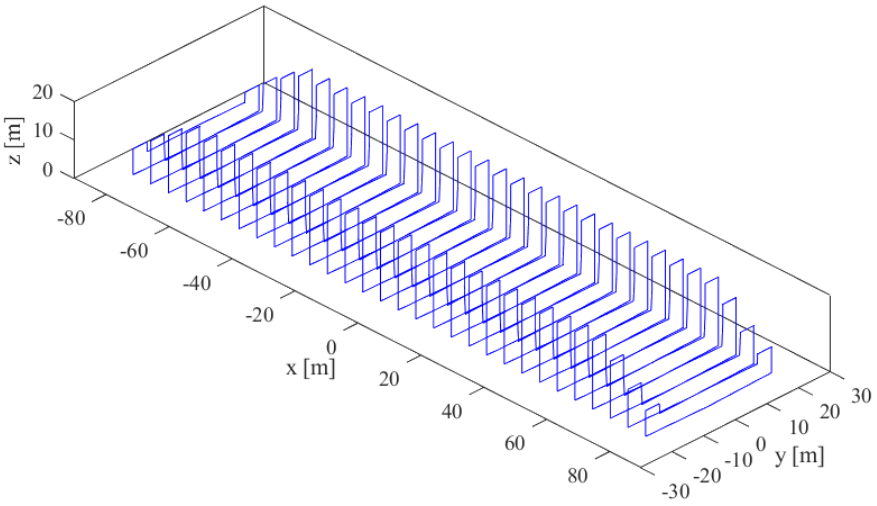

Figure 4.4. Hydrostatic sections of a floating dock (taking 30 sections for example).

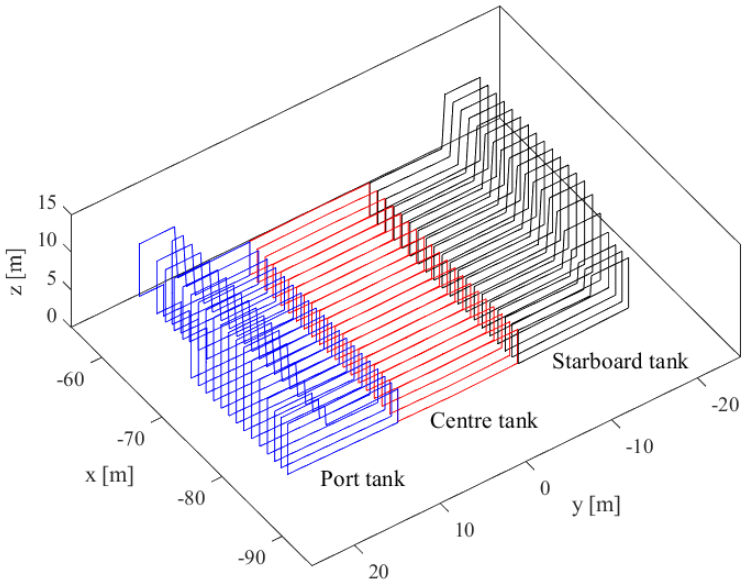

Figure 4.5. Hydrostatic sections of the port, center, and starboard tanks (taking 20 sections for example).

The hydrostatic loads acting on the 3D body are calculated by integrating the hydrostatic forces acting on the 2D sections along the longitudinal direction of the dock and the ballast tanks. The geometries of the 2D sections' submerged region are expressed using N number of points $(y_k,\ z_k)$ on the boundaries. The formulas of a section's area, the first and

second moments of area are given in Table 4.3, where $\bar{y}_{1,k} = 0.5(y_k + y_{k+1})$, $\bar{z}_{1,k} = 0.5(z_k + z_{k+1})$, $\bar{y}_{2,k} = 0.5(y_k^2 + y_{k+1}^2)$, $\bar{z}_{2,k} = 0.5(z_k^2 + z_{k+1}^2)$, $\bar{y}_{3,k} = 0.5[(y_k - y_{\mathrm{CG}})^2 + (y_{k+1} - y_{\mathrm{CG}})^2]$, $\bar{z}_{3,k} = 0.5[(z_k - z_{\mathrm{CG}})^2 + (z_{k+1} - z_{\mathrm{CG}})^2]$, $\Delta y_k = y_{k+1} - y_k$ and $\Delta z_k = z_{k+1} - z_k$. The areas of sections A are used to calculate the displaced water of the dock (or vessel) and the volume of the ballast water by integrating along the longitudinal direction. The centroid of the submerged region (y_0, z_0) are computed using the equations of $y_0 = S_z/A$ and $z_0 = S_y/A$. I_y and I_z are to calculate the mass moment of inertia of the ballast water in Equation (4.2).

Table 4.3. Formulas and discretization of the areas, the first moments and second moments of area.

Variables	Surface integral	Line integral	Discretization
A	$\iint \mathrm{d}y\mathrm{d}z$	$\oint -\mathrm{z}\mathrm{d}y$	$\sum_{k=1}^{N} -\bar{z}_{1,k}\,\Delta y_k$
S_y	$\iint z\mathrm{d}y\mathrm{d}z$	$-\frac{1}{2}\oint \mathrm{z}^2\mathrm{d}y$	$-\frac{1}{6}\sum_{k=1}^{N}(2\bar{z}_{1,k}^2 + \bar{z}_{2,k})\,\Delta y_k$
S_z	$\iint y\mathrm{d}y\mathrm{d}z$	$\frac{1}{2}\oint y^2\mathrm{d}z$	$\frac{1}{6}\sum_{k=1}^{N}(2\bar{y}_{1,k}^2 + \bar{y}_{2,k})\,\Delta z_k$
I_y	$\iint (z - z_{CG})^2\mathrm{d}y\mathrm{d}z$	$-\frac{1}{3}\oint (\mathrm{z} - \mathrm{z}_{CG})^3\mathrm{d}y$	$-\frac{1}{3}\sum_{k=1}^{N}(\bar{z}_{1,k} - z_{CG})\,\bar{z}_{3,k}\Delta y_k$
I_z	$\iint (y - y_{CG})^2\mathrm{d}y\mathrm{d}z$	$\frac{1}{3}\oint (y - y_{CG})^3\mathrm{d}z$	$\frac{1}{3}\sum_{k=1}^{N}(\bar{y}_{1,k} - y_{CG})\,\bar{y}_{3,k}\Delta z_k$

It should be noted that the immersed region of the body is determined based on the dock's draught, the heel, and trim angles. The dock's draught, the heel and trim angles, and the sea water level are known when calculating the dock's hydrostatic loads. However, the

height of the water level in a ballast tank is unknown. It can be calculated using a secant iteration method of a single point. Once the ballast water volume in a tank is updated, the water level can be obtained using Equation (4.8).

$$h^{(n+1)} = h^{(n)} - \frac{h^{(n)} - h_{\text{pre}}}{V^{(n)} - V_{\text{pre}}}(V^{(n)} - V) \tag{4.8}$$

where *n* is the iteration index, V is the given water volume in a ballast tank, h_{pre} is the water level height in the previous time step, and V_{pre} is the water volume for the water level h_{pre}.

4.2.4 Hydrodynamic force model

The hydrodynamic force model is used to calculate the added mass and damping of the floating dock and the docked vessel in heave, roll, and pitch. The added mass and mass moment of inertia of the floating dock are shown in Table 4.4. These formulas are obtained by integrating the added mass and mass moments of inertia of a 2D plate along the longitudinal direction of the dock and incorporating a 3D correction using the aspect-ratio formula of Pabst [30]. The surge, sway, and yaw components are neglected in the present model due to their relatively small magnitudes compared to the heave, roll, and pitch components.

$$\Psi(B/L) = \frac{1}{\sqrt{1 + (B/L)^2}}\left(1 - \frac{0.425B/L}{1 + (B/L)^2}\right) \tag{4.9}$$

Table 4.4. Formulas and results of added mass and mass moment of inertia.

Motion	Formula	Value
Heave	$m_{33\text{added}} = \frac{1}{8}\rho\pi B^2 L\Psi(B/L)$	9.4604×10^7 kg
Roll	$I_{11\text{added}} = \frac{1}{256}\rho\pi B^4 L\Psi(B/L)$	4.6830×10^9 kg · m^2
Pitch	$I_{22\text{added}} = \frac{1}{96}\rho\pi B^2 L^3\Psi(B/L)$	2.2378×10^{11} kg · m^2

In the dynamic damping model, the damping coefficients are calculated using the mass matrix of the dock (vessel), a damping ratio of 5%, and natural frequencies of the heave, roll, and pitch motions of the dock (vessel). The natural frequencies are calculated using Equations (4.10) – (4.12) [31].

$$\omega_{\text{heave}} = \sqrt{\frac{\rho A_w \text{g}}{m_{33}}} \tag{4.10}$$

$$\omega_{\text{roll}} = \sqrt{\frac{\rho \text{g} \nabla \overline{GM}_\text{r}}{I_{11}}} \tag{4.11}$$

$$\omega_{\text{pitch}} = \sqrt{\frac{\rho \text{g} \nabla \overline{GM}_\text{p}}{I_{22}}} \tag{4.12}$$

where m_{33}, I_{11} and I_{22} include the contributions of the dock, ballast water, and dock's added mass. Only heave, roll, and pitch components are considered. $\overline{GM}_\text{r}$ and $\overline{GM}_\text{p}$ are the transverse and longitudinal metacentric heights, respectively. Free surface effects inside the ballast tanks are neglected. In Figure 4.6, the restoring coefficients in heave, roll, and pitch are

shown at different draughts of the dock, which provide the damping coefficients using Equations (4.10) – (4.12).

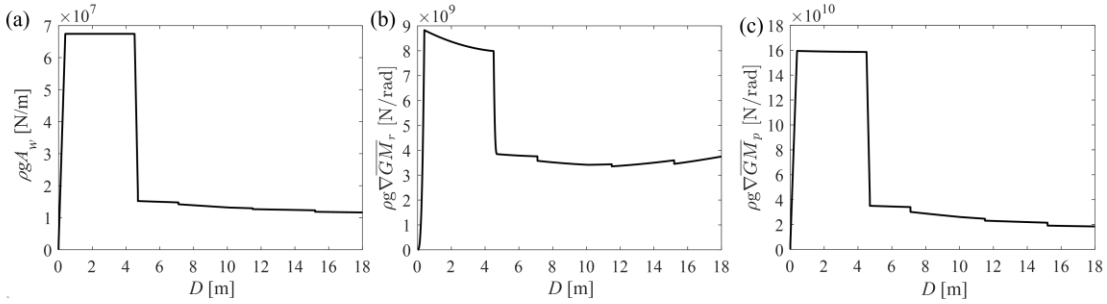

Figure 4.6. Hydrostatic restoring coefficients in heave, roll, and pitch motions at different draughts.

4.2.5 Hydraulic model of the ballast water system

The ballast water system schematic is presented in Figure 4.7. The floating dock is equipped with six ballast pumps that are responsible for pumping the water in three tanks from port to starboard. The pipes connected to the tanks have a diameter of 400 mm, while the main pipe has a diameter of 600 mm. All the tanks, including the port, center, and starboard tanks, are equipped with their own butterfly valves. The inlet and outlet valves are located on the main pipes and are used for ballasting and de-ballasting operations, respectively. Additionally, a connection pipe, which has a diameter of 400 mm and a connection valve, is used to connect the pipe network of one pump to that of other pumps.

During de-ballasting, the port, center, starboard, and outlet valves are open while the inlet and connection valves are closed. Conversely, during ballasting, the inlet valves are open while the outlet valves are closed. The hydraulic calculations of the ballast water system are based on the pressure changes of different components, including pipes, valves, and pumps. The changes in the water head (representing the pressure drop) along the pipes are neglected, while the changes in the water heads due to the valves and pumps are considered. The water head changes caused by the outlet, port, center, and starboard valves are calculated using Equations (4.13) – (4.16).

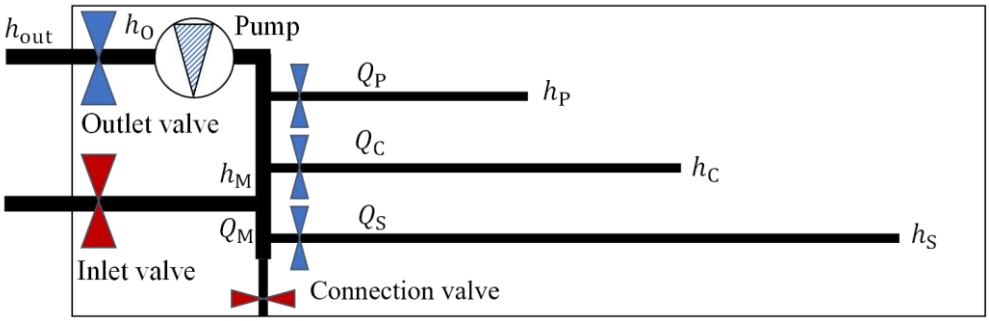

Figure 4.7. Schematic of the ballast water system.

$$h_{\mathrm{O}} - h_{\mathrm{out}} = \lambda_{\mathrm{M}} |Q_{\mathrm{M}}| Q_{\mathrm{M}} \tag{4.13}$$

$$h_{\mathrm{P}} - h_{\mathrm{M}} = \lambda_{P} |Q_{\mathrm{P}}| Q_{\mathrm{P}} \tag{4.14}$$

$$h_{\mathrm{C}} - h_{\mathrm{M}} = \lambda_{\mathrm{C}} |Q_{\mathrm{C}}| Q_{\mathrm{C}} \tag{4.15}$$

$$h_{\mathrm{S}} - h_{\mathrm{M}} = \lambda_{\mathrm{S}} |Q_{\mathrm{S}}| Q_{\mathrm{S}} \tag{4.16}$$

where h_{M}, h_{P}, h_{C}, h_{S}, and h_{O} are the water heads at the right sides of the pump, port, center, starboard, and outlet (inlet) valves in Figure 4.7, and h_{out} is the water head at the left side of the outlet valve. Q_{M}, Q_{P}, Q_{C} and Q_{S} are the flow rates in the main, port, center, and starboard pipes. The coefficients λ_{M}, λ_{P}, λ_{C} and λ_{S} are given by the K_V values of the butterfly valves, as shown in Table 4.5. The K_V value is the volume of water (measured in m^3) that will pass through the valve in one hour at a pressure drop of 1 bar. The K_V values depend on the valve opening angles and are given by experimental measurements of the butterfly valves **¡Error! No se encuentra el origen de la referencia.**. The expression of λ can be written as Equation (4.17).

$$\lambda = \frac{1}{\mathrm{g}(\mathrm{KV}/36000)^2} \quad [\mathrm{s}^2/\mathrm{m}^5] \tag{4.17}$$

Table 4.5. K_V values of different opening angles for the butterfly valves [27].

θ [deg]	20	30	40	50	60	70	80	90
KV of 400 mm	155	475	105	1880	3150	5250	9450	10500
KV of 600 mm	375	1125	2500	4500	7500	12550	22500	25000

The water head of pumps is calculated using Equation (4.18).

$$h_{\mathrm{O}} - h_{\mathrm{M}} = h_0 - \lambda_{\mathrm{pump}} |Q_{\mathrm{M}}| Q_{\mathrm{M}} \tag{4.18}$$

where $h_0 = 21.25\ \mathrm{m}$ is the pump's total water head with zero flow rate and $\lambda_{\mathrm{pump}} = 20\ \mathrm{s}^2/\mathrm{m}^5$ is the pump coefficient. The continuity equation between the main pipe and the branch pipes is given by Equation (4.19).

$$Q_{\mathrm{M}} = Q_{\mathrm{P}} + Q_{\mathrm{C}} + Q_{\mathrm{S}} \tag{4.19}$$

By substituting Equations (4.13) - (4.16) and (4.18) into Equation (4.19), the water head h_{M} is calculated using an iterative formula in Equation (4.20).

$$h_{\mathrm{M}}^{(n+1)} = \frac{\Omega_{\mathrm{P}}^{(n)} h_{\mathrm{P}} + \Omega_{\mathrm{C}}^{(n)} h_{\mathrm{C}} + \Omega_{\mathrm{S}}^{(n)} h_{\mathrm{S}} + \Omega_{\mathrm{M}}^{(n)} (h_0 - h_{\mathrm{out}})}{\Omega_{\mathrm{P}}^{(n)} + \Omega_{\mathrm{C}}^{(n)} + \Omega_{\mathrm{S}}^{(n)} + \Omega_{\mathrm{M}}^{(n)}} \tag{4.20}$$

where n is the iteration index, and $\Omega_{\mathrm{P}}^{(n)}$, $\Omega_{\mathrm{C}}^{(n)}$, $\Omega_{\mathrm{S}}^{(n)}$ and $\Omega_{\mathrm{M}}^{(n)}$ are calculated using Equation (4.21).

$$\begin{aligned}
\Omega_{\mathrm{P}}^{(n)} &= \left[\lambda_{\mathrm{P}}\left(h_{\mathrm{P}} - h_{\mathrm{M}}^{(n)}\right)\right]^{-1/2} \\
\Omega_{\mathrm{C}}^{(n)} &= \left[\lambda_{\mathrm{P}}\left(h_{\mathrm{C}} - h_{\mathrm{M}}^{(n)}\right)\right]^{-1/2} \\
\Omega_{\mathrm{S}}^{(n)} &= \left[\lambda_{\mathrm{P}}\left(h_{\mathrm{S}} - h_{\mathrm{M}}^{(n)}\right)\right]^{-1/2} \\
\Omega_{\mathrm{M}}^{(n)} &= \left[\left(\lambda_{\mathrm{O}} + \lambda_{\mathrm{pump}}\right)\left(h_{\mathrm{O}} - h_{\mathrm{out}} + h_{\mathrm{M}}^{(n)}\right)\right]^{-1/2}
\end{aligned} \tag{4.21}$$

The initial value of h_M during the iteration is given as the convergent result of the previous time step, while the initial value at the first time step is chosen as $0.5h_{\mathrm{out}}$. For the ballasting operation, the solution is given by taking $h_0 = 0$ and $\lambda_{pump} = 0$. Once the flow rate of a ballast tank is obtained, the ballast water volume is updated using Equation (4.22).

$$\frac{\mathrm{d}\alpha_j}{\mathrm{d}t} = \frac{Q_j}{V_{\mathrm{max},j}} \tag{4.22}$$

where α_j is the volume fraction of the water in the j^{th} ballast tank, $V_{\mathrm{max},j}$ is the total volume of the j^{th} tank and Q_j is the corresponding flow rate.

4.2.6 Modified P-controller for the ballast control system

The primary objective of a ballast control system is to ensure the stability of the dock and vessel during docking operations. This involves controlling the pitch and roll angles within allowable ranges. To achieve this, the valve opening angles of the port and starboard tanks are chosen as control objects. The valves of the side tanks are typically divided into four groups, and the opening angle of each group of the valves serves as a control signal given as in Equation (4.23).

$$\theta_{\text{target},i}^{(n)} = \theta_{max}\min\{1 + K_p^{(n)} c_{p,i} L\psi + K_r^{(n)} c_{r,i} B\gamma, 1\} \tag{4.23}$$

where

$$K_p^{(n)} = \begin{cases} K, & |\psi| > \psi_{upper} \\ 0, & |\psi| < 0.1\psi_{upper} \\ K_p^{(n-1)}, & \text{otherwise} \end{cases} \tag{4.24}$$

$$K_r^{(n)} = \begin{cases} K, & |\gamma| > \gamma_{upper} \\ 0, & |\gamma| < 0.1\gamma_{upper} \\ K_r^{(n-1)}, & \text{otherwise} \end{cases} \tag{4.25}$$

Here K is the total control coefficient. n represents the present time step and n-1 represents the previous time step. The pitch and roll control coefficients for various groups of control objects during the ballasting operation are shown in Table 4.6, while those of the de-ballasting operation have opposite signs. The ballasting and de-ballasting operations thus have inverse control effects. The value of $\theta_{\text{target},i}^{(n)}$ needs to be corrected as 0 when Equation (4.23) provides a negative value. K and $\theta_{\max}$ are critical for the control of the dock's motions. The effects of the control parameters on the control performance will be studied in Section 4.3.2.

Table 4.6. Pitch and roll control coefficients for the ballasting operation.

Control objects of the valves	No.1-3	No.4-6	No.13-15	No.16-18
Pitch control coefficient $c_{p,i}$	-1	1	-1	1
Roll control coefficient $c_{r,i}$	-1	-1	1	1

The pitch and roll angles are given based on the draughts at the dock's four corners (D_1, D_2, D_3, D_4), as expressed in Equations (4.26) - (4.27). The positions of the four corners are shown in Table 4..

$$\psi = \arctan\frac{D_1 - D_3}{L} \tag{4.26}$$

$$\gamma = \arctan\frac{D_4 - D_2}{B} \tag{4.27}$$

Table 4.7. Position of four corners of the dock.

Corner number	1	2	3	4
x (m)	84.24	0	-84.24	84.24
y (m)	19.9	19.9	19.9	-19.9
z (m)	3.2	3.2	3.2	3.2

The target valve opening angle in each tank is calculated using Equation (4.23). However, it should be noted that the valve mechanics have limitations that prevent the actual opening angle from immediately reaching the target angle. Therefore, there may be a delay between the calculation of the target angle and the actual opening angle of the valve. The present valve opening angle $\theta_{\text{present},i}$ is updated based on the strategy presented in Equation (4.28).

$$\theta_{\text{present},i}^{(n+1)} = \begin{cases} \theta_{\text{present},i}^{(n)} + \Delta t\omega_{\text{valve}}, \theta_{\text{present},i}^{(n)} < \theta_{\text{target},i}^{(n)} - \Delta t\omega_{\text{valve}} \\ \theta_{\text{present},i}^{(n)} + \Delta t\omega_{\text{valve}}, \theta_{\text{present},i}^{(n)} > \theta_{\text{target},i}^{(n)} + \Delta t\omega_{\text{valve}} \\ \theta_{\text{present},i}^{(n)}, \text{otherwise} \end{cases} \tag{4.28}$$

where $\omega_{\text{valve}} = 90$ deg/min is the angular velocity of the valve and Δt is the time step.

The target valve angles will be updated every $\Delta T = N_T \Delta t$, using Equations (4.24) - (4.25). If these conditions are not met, the target angles are kept the same as in the previous time step to prevent frequent changes in the control signals. To balance the controls in the pitch and roll motions, a control range is defined as $\Delta D = L\psi_{upper} = B\gamma_{upper}$. The effects of ΔT and ΔD on the control performance of the present modified P-controller will be discussed in Section 4.3.2.

The workflow of the automatic control algorithm for the floating dock is presented in Figure 4.8. First, the modified P-controller calculates the valve opening angles for the ballast tanks. Next, the hydraulic model is utilized to compute the flow rates and update the water volumes in the ballast tanks. Then, the hydrostatic and hydrodynamic forces are calculated. Using the 6-DOF model, the dock's heave, pitch, and roll motions are calculated. These motions are fed back to the modified P-controller, which then determines the valve opening angles for the next time step.

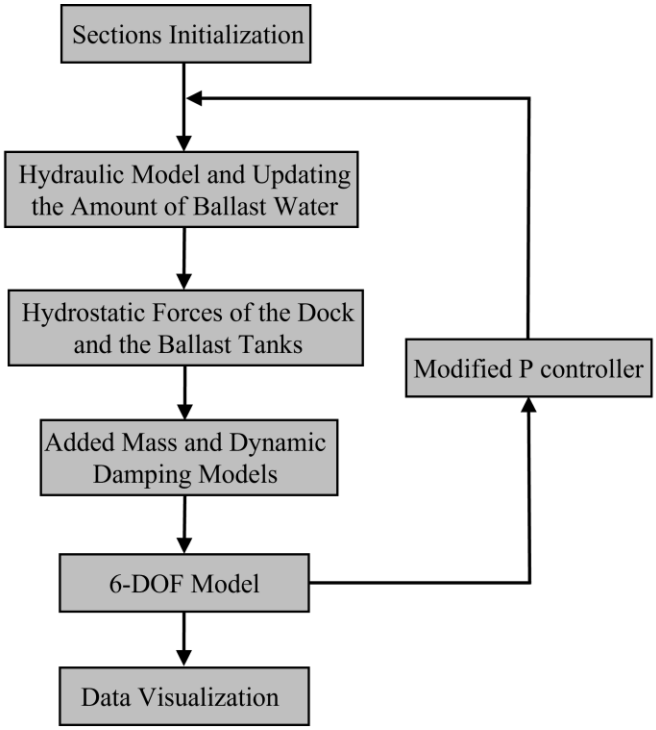

Figure 4.8. Workflow of the present algorithm for the automatic control of a floating dock.

4.3 Results and Discussion

The present study involves four branches of load cases, including gravitational ballasting and de-ballasting using pumps, with parameters listed in Table 4.8. In Section 4.3.1, Case 1 examines the dynamic process of the de-ballasting operation for a floating dock, with a time-step sensitivity study and a numerical stability analysis of the hydraulic model. Section 4.3.2 presents Case 2, which explores the effects of different control parameters on the control performance during de-ballasting. Cases 3 and 4, detailed in Section 4.3.3, evaluate the performance of the present control parameters in gravitational ballasting cases. Overall, these load cases provide insight into the performance of the proposed automatic ballast control system and its potential benefits for improving the stability of floating docks during various operations.

Table 4.8. Load cases of the present study.

Case	1	2	3	4
Operation	De-ballasting	De-ballasting	Ballasting	Ballasting
Control	No controller	Modified P-controller	No controller	Modified P-controller
h_0	0	21.25 m	0	21.25 m
c_{pump}	0	$20\ \text{s}^2/\text{m}^5$	0	$20\ \text{s}^2/\text{m}^5$

4.3.1 Time-step sensitivity study and numerical stability analysis of the hydraulic model

The grid sensitivity of section number and point number of the sections for the dock and the ballast tanks, as well as the convergence study of the water level in ballast tanks, are given in the study of Zhang et al. [13]. The dock is sliced into 150 sections, while each tank is sliced into 20 sections. The number of points for a dock's section is 18 and those of port, center, and starboard tanks are 8, 8, and 6, respectively. All the section numbers and point numbers are chosen the same as those in the study of Zhang et al. [13].

The time-step sensitivity of the draught, pitch, and roll angles of Case 1 is performed and shown in Figure 4.9. Three different time steps of $\Delta t = 1\ \text{s},\ 0.5\ \text{s}$ and $0.25\ \text{s}$ are adopted,

and the results match well with each other. Therefore, the time step of $\Delta t = 1$ s is used for further calculations to reduce the computational cost.

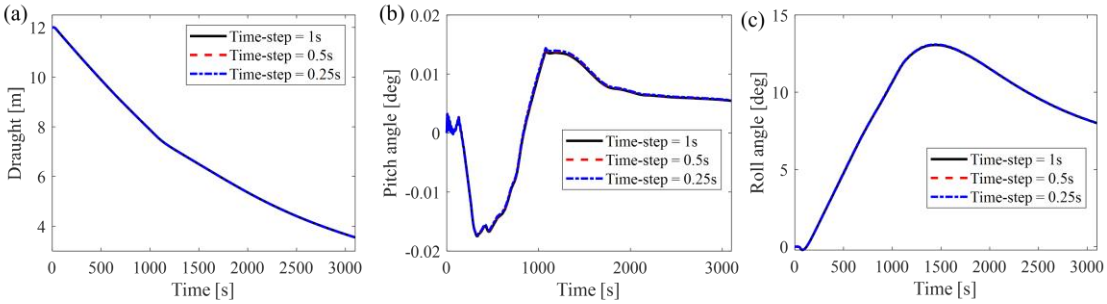

Figure 4.9. Time-step sensitivity study of the draught, pitch, and roll angles in Case 1.

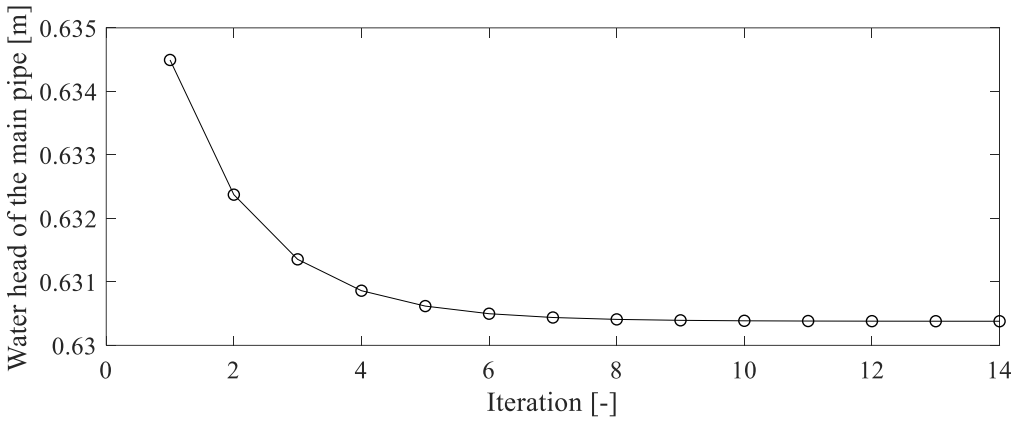

Figure 4.10. Iteration of the water head of the first main pipe at 1000s in Case 1.

The numerical stability of the hydraulic model is also studied. Figure 4.10 shows an iteration of the water head of the first main pipe (connecting No. 1, 7, and 13 ballast tanks) at $t = 1000$ s in Case 1. The water head converges within 14 steps, demonstrating the stability of the numerical scheme. The iterations of the water heads of other pumps and at different time steps are similar to that in Figure 4.10.

4.3.2 Automatic control study of the de-ballasting operation

In Figure 4.9, an excessive roll angle is induced without controlling the opening angles of valves, which could potentially cause stability issues and disrupt the operation of the floating dock. To prevent such scenarios, an automatic ballast control is necessary to maintain the roll and pitch angles within safe ranges. This section examines the performance of the ballast control system and investigates the effects of various control parameters, including the valve's angular speed ω_{valve}, the control range ΔD, the maximum valve opening angle $\theta_{\max}$, the total control coefficient K and the control duration number N_T, to optimize the control inputs and ensure safe and efficient operation.

(I) Simulation of a designed reference case

To facilitate comparisons between different control parameters, a reference case with predefined values is designed. This reference case serves as a baseline for evaluating the effectiveness of various control inputs and enables us to identify the optimal values for each parameter. The reference case includes an angular speed of the valves of 1.5 deg/s, a control range ΔD of 0.04 m, a maximum valve opening angle $\theta_{\max}$ of 90 deg for draught less than 4.5 m and 70 deg for draught larger than 4.5 m, a total control coefficient K of 1, and a control duration number N_T of 5.

Figure 4.11 shows the pitch and roll angles during the de-ballasting process using a modified P-controller in Case 2 with the abovementioned parameters. The dock submerges from an initial draught of 12m and gradually reaches a working draught of 3.5 m at around 3000 s. In [0, 3000] s, the pitch and roll angles exhibit small oscillations with maximum values of $|\psi|_{max} = 0.016$ deg and $|\gamma|_{max} = 0.0783$ deg, respectively. The corresponding draught differences caused by the maximum pitch and roll motions are denoted as $L|\psi|_{max}$ and $B|\gamma|_{max}$. For the reference case, the values are $L|\psi|_{max} = 0.0471$ m and $B|\gamma|_{max}. = 0.0544$ m, indicating that the roll motion contributes to a larger draught difference than the pitch motion.

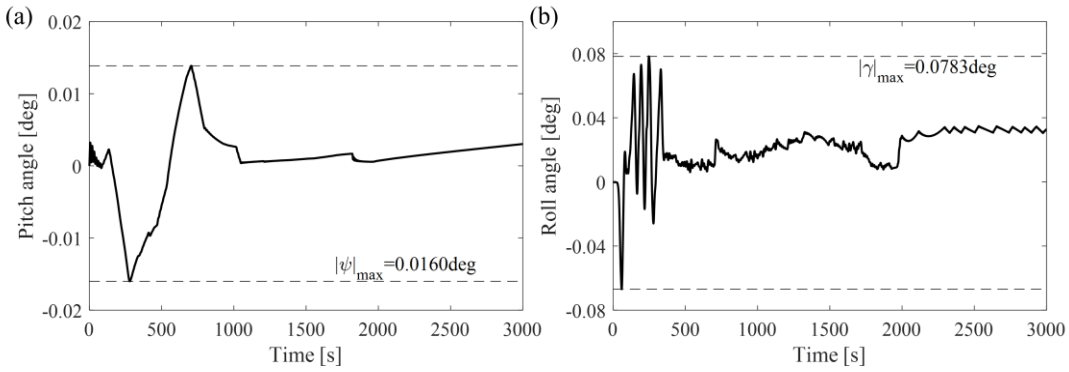

Figure 4.11. Pitch and roll angles during the ballasting using a modified P-controller in Case 2.

Figure 4.12 shows the comparisons between the target and present opening angles of Valve No. 01. It can be seen that the present valve angle can roughly follow the target valve angle, although there is a delay due to the limitation of the valve's angular speed. Figure 4.13 shows the comparisons of the valve opening angles between Valves No. 01, 06, and 13. The valve angles of Valves No. 01 and 06 are the same in [0, 264] s and [1045, 3000] s but different in [264, 1045] s. It means the pitch control is active in [264, 1045] s, which results in the difference in the flow rate in Figure 4.14. The flow rate responds correctly to the changing of the valve opening angle in this pitch control. However, the results of the roll control observed from the comparison of Valves No. 01 and 13 are different. It is because the water level in the global coordinate system in the tank also affects the flow rate. The water levels in the global coordinate system in Tank No. 01 and 13 are different due to the asymmetric distribution of the ballast tank. The total flow rates through Pumps No.01 to 06 are shown in Figure 4.15. In the beginning, these total flow rates rise quickly from 0 to 0.95 m^3/s. Then, the total flow rates through all the pumps are controlled within a range of [0.85, 1] m^3/s. The range is higher than the value of 0.75 m^3/s, which is the pump capacity at a working water head difference of 10m. The water head difference in this case is always less than 10 m, and the total flow rates are larger than the capacity value.

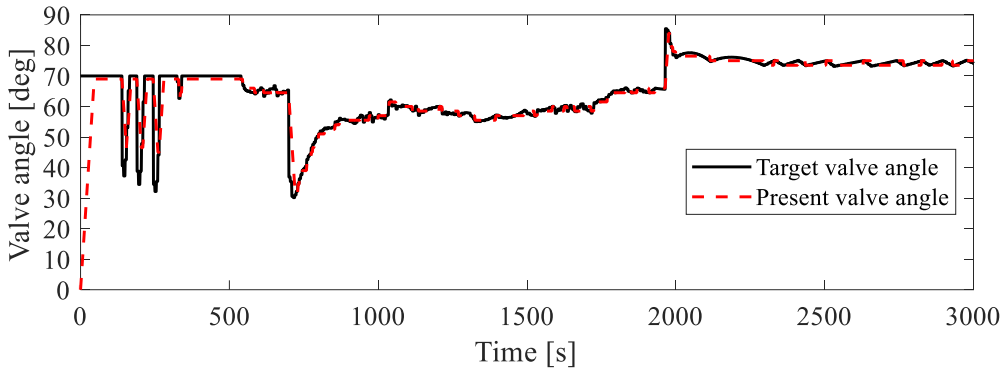

Figure 4.12. Target and present opening angles of Valve No.01 in Case 2.

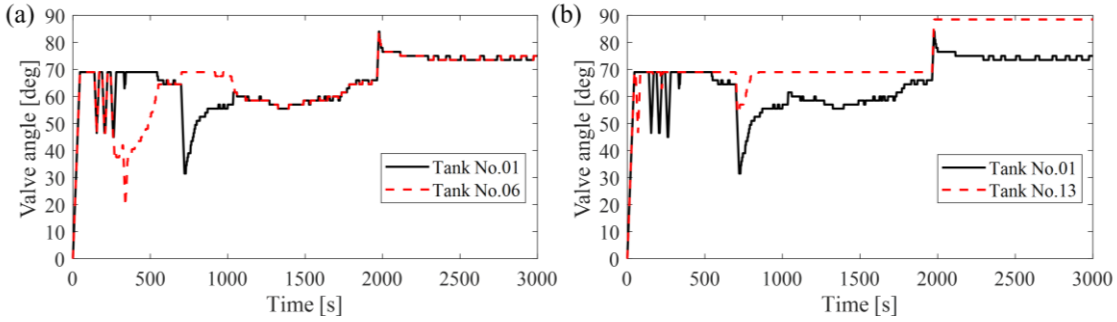

Figure 4.13. Comparisons of the valve opening angles between Valves No.1, 6, and 13 in Case 2.

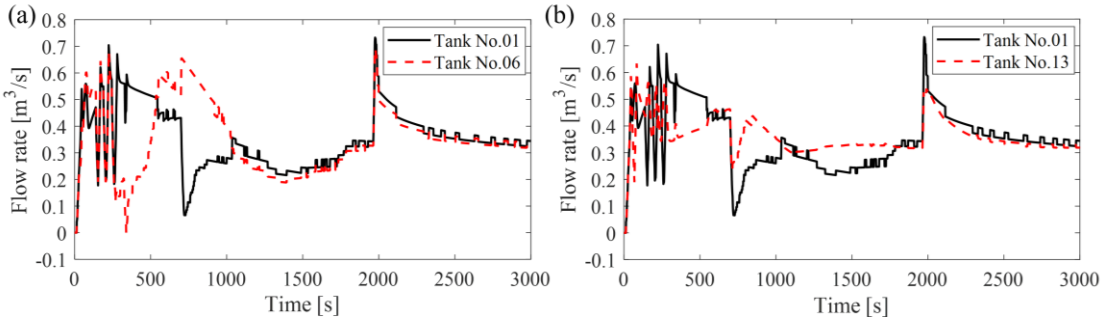

Figure 4.14. Comparisons of the flow rates between Valves No. 01, 06, and 13 in Case 2.

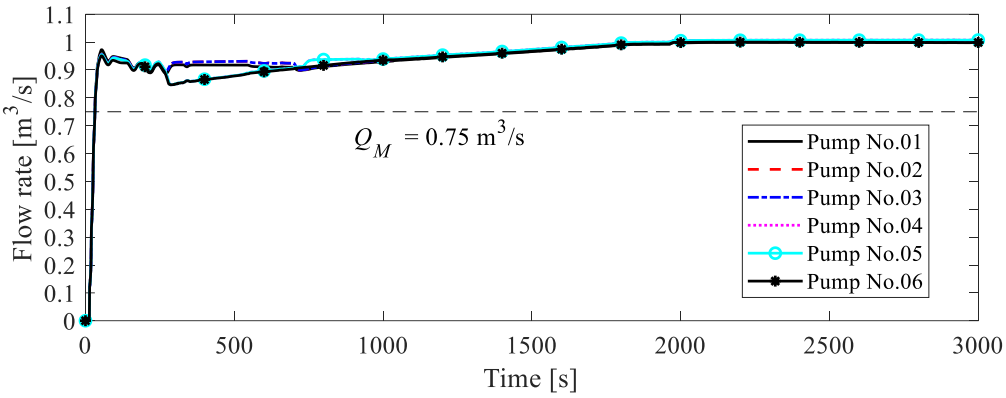

Figure 4.15. Flow rates of Pumps No.01 to No.06 during the de-ballasting using the modified P-controller in Case 2.

The dock's vertical velocity during the de-ballasting using the modified P-controller in Case 2 is shown in Figure 4.16. As the valves open, the vertical velocity increases gradually and reaches a peak value of 4.68 mm/s. However, at 1823 s the pontoon deck emerges, resulting in a sudden increase in the waterplane and a sharp decline in the dock's vertical velocity. To further illustrate this phenomenon, Figure 4.17 also displays the waterplanes at the draughts of 4 m and 10.1 m. The increase in the waterplane area can significantly reduce the dock's vertical velocity.

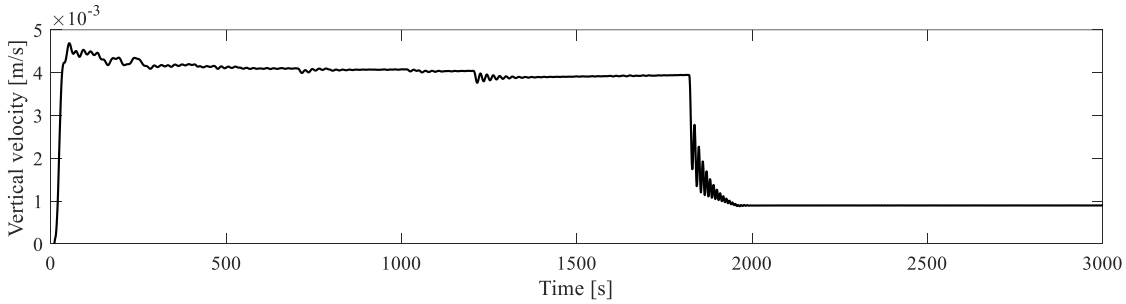

Figure 4.16. Dock's vertical velocity during de-ballasting with the modified P-controller in Case 2.

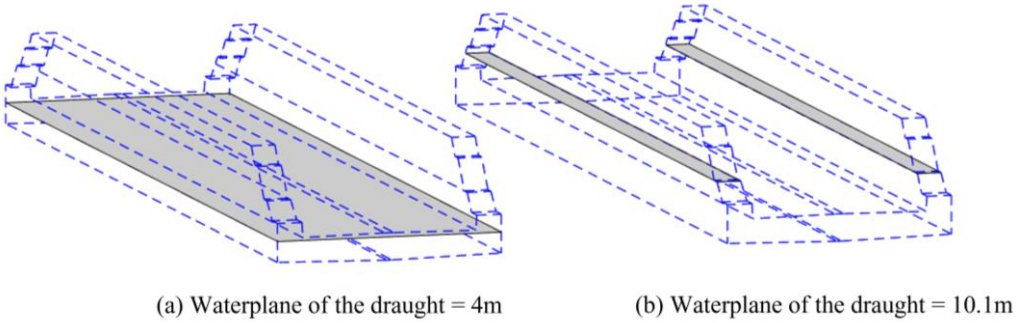

Figure 4.17. Waterplanes at draughts of 4 m and 10.1 m.

The maximum values of the pitch angle $|\psi|_{\max}$ and roll angle $|\gamma|_{\max}$ during the operations using automatic control are important indicators of the control performance of the automatic control. In Section 4.3.2 (II), similar indicators, namely the maximum differences of the draughts due to the maximum pitch and roll angles, $L|\psi|_{\max}$ and $B|\gamma|_{\max}$, are adopted to show the control performance of the pitch and roll motions together. These indicators enable a comprehensive assessment of the control performance of both pitch and roll motions and facilitate their comparison.

(II) Effects of the control parameters

1) Angular speed of the valves

Figure 4.18 shows the values of $L|\psi|_{\max}$ and $B|\gamma|_{\max}$ of the dock with different angular speeds of valves. The results indicate a decreasing trend in the maximum draught differences due to pitch and roll motions as the angular speed of valves increases. This trend suggests that a higher angular speed of valves can improve the control performance of the automatic control system. However, the real angular speed of valves is 1.5 deg/s, and a higher angular speed requires an increase in device cost. Therefore, a balance between the control performance and the device cost should be achieved.

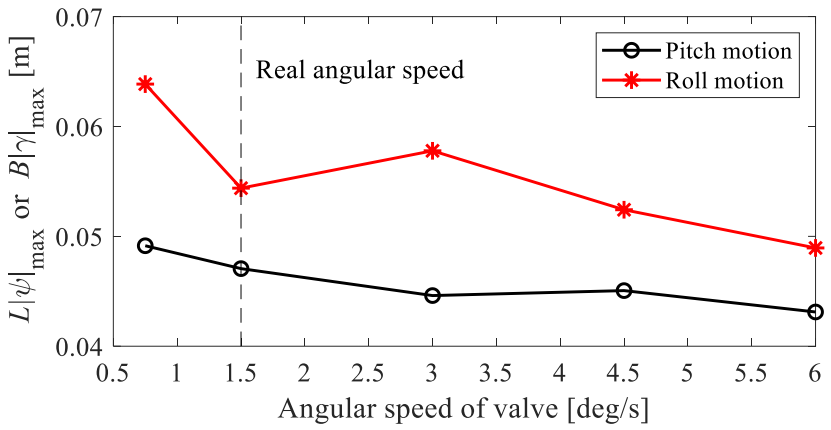

Figure 4.18. $L|\psi|_{\max}$ and $B|\gamma|_{\max}$ of the dock with different angular speeds of valves.

2) Control ranges of pitch and roll angles

The time histories of the draught differences due to the roll motion with different control ranges ΔD are shown in Figure 4.19. When using small control ranges ΔD in Figures 19 (a)-(b), the results are similar to the time history of the roll angle in Figure 4.11. However, when using large control ranges ΔD in Figure 4.19 (c)-(d), the duration of the oscillation with a large amplitude extends, and the amplitude increases. The values of $L|\psi|_{\max}$ and $B|\gamma|_{\max}$ of different control ranges are shown in Figure 4.20, indicating that the values of $L|\psi|_{\max}$ and $B|\gamma|_{\max}$ show a roughly linear increase with the increasing control ranges. Therefore, to achieve optimal control performance, a small control range should be adopted.

3) Maximum valve angle

To reduce the amplitudes of the pitch and roll angle oscillations, a smaller maximum valve angle, less than 90 deg, is used in Equation (4.23) when the draught of the dock exceeds 4.5 m. As shown in Figure 4.21, the values of $L|\psi|_{\max}$ and $B|\gamma|_{\max}$ for the cases using different maximum valve angles are compared. It is observed that $L|\psi|_{\max}$ and $B|\gamma|_{\max}$ are both minimized when $\theta_{\max} = 65$ deg and 70 deg. Therefore, when the draught of the dock is larger than 4.5 m, the maximum valve angle should be selected between 65 deg and 70 deg to achieve optimal control performance.

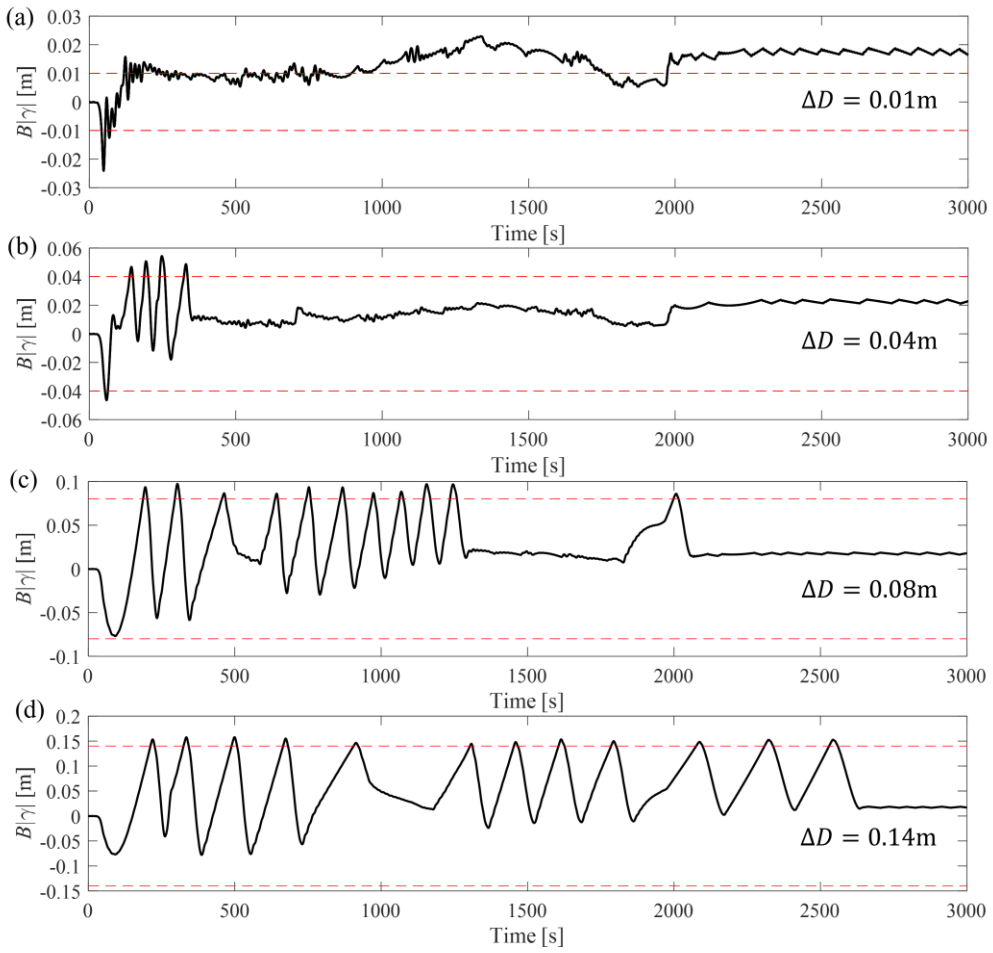

Figure 4.19. Time histories of the draught differences due to the roll motion using different control ranges.

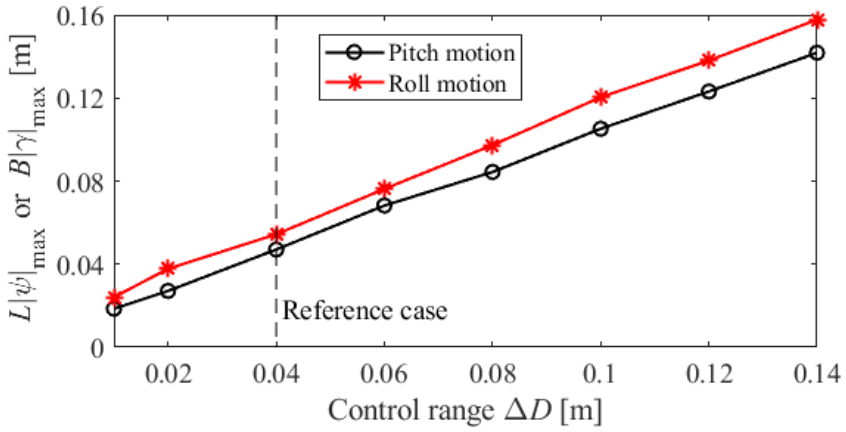

Figure 4.20. $L|\psi|_{\max}$ and $B|\gamma|_{\max}$ of different control ranges.

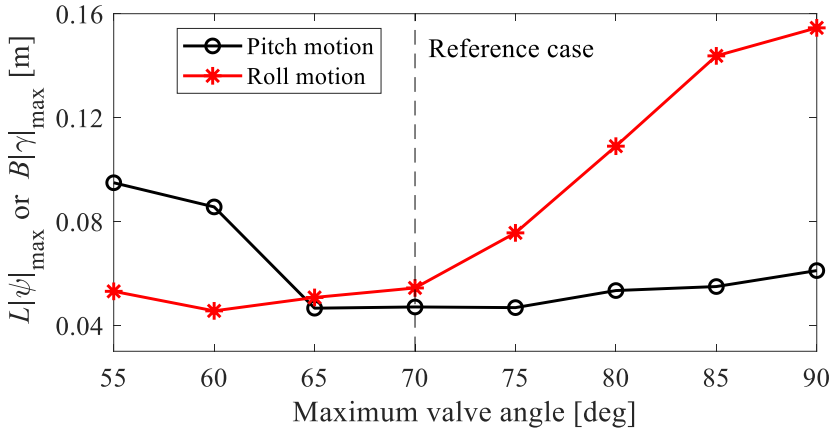

Figure 4.21. $L|\psi|_{\max}$ and $B|\gamma|_{\max}$ of different maximum valve angles when the draught is larger than 4.5 m.

4) Total control coefficient

Figure 4.22 displays the values of $L|\psi|_{\max}$ and $B|\gamma|_{\max}$ for the cases using different total control coefficients K. It can be observed that for K values in the range of [0.4, 2], the maximum differences in draught due to pitch and roll motions are similar. This indicates that the control performance is not significantly affected by the total control coefficients K within this range.

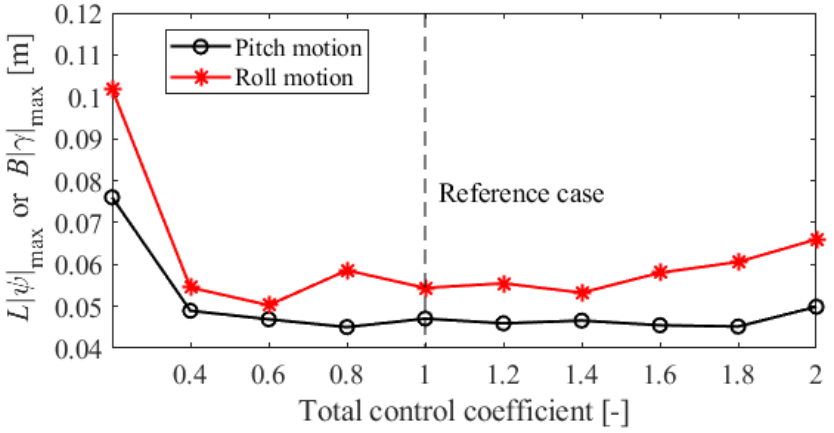

Figure 4.22. $L|\psi|_{\max}$ and $B|\gamma|_{\max}$ of different total control coefficients.

5) Control duration number

Figure 4.23 shows increasing trends of $L|\psi|_{\max}$ and $B|\gamma|_{\max}$ with the increasing control duration number. when $N_T \geq 10$, the maximum draught differences due to the pitch and roll motions have a rapid increase. Therefore, it is recommended to choose a control duration number in a range of [1, 10] to prevent such an increase in maximum draught differences.

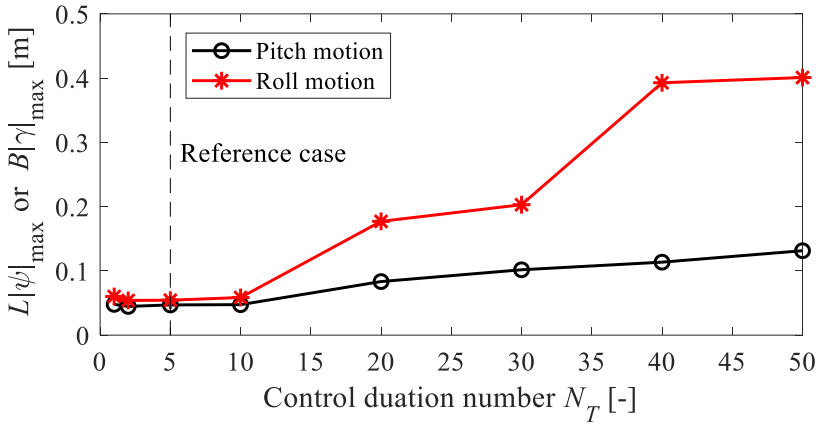

Figure 4.23. $L|\psi|_{\max}$ and $B|\gamma|_{\max}$ of different control duration numbers.

After conducting a comprehensive parameter study, it can be concluded that the modified P-controller is capable of maintaining robust control performance over a wide range of different parameters. In the reference case, the maximum draught differences resulting from pitch and roll motions are found to be 0.0471 m and 0.0544 m, respectively. These promising results pave the way for further investigation into the control parameters of the reference case, which will be studied in the gravitational ballasting cases in Section 4.3.3.

4.3.3 Automatic control study of the ballasting operation

Figure 4.24 shows the draught, pitch, and roll angles during the ballasting without the controller in Case 3, where the maximum roll angle reaches 8.9 deg, posing a potential risk to the vessel docking operations. To prevent this risk, the present modified P-controller using the control parameters of the reference case in Section 4.3.2 (I) is employed to stabilize the

pitch and roll angles, as shown in Figure 4.25. With this controller, the pitch and roll angles are maintained not larger than 0.0145 deg and 0.0604 deg, respectively. The maximum draught differences due to the pitch and roll motions are 0.0425 m and 0.0419 m, respectively, which are negligible during vessel docking operations. Thus, the present modified P-controller proves to be effective in stabilizing the ballasting process.

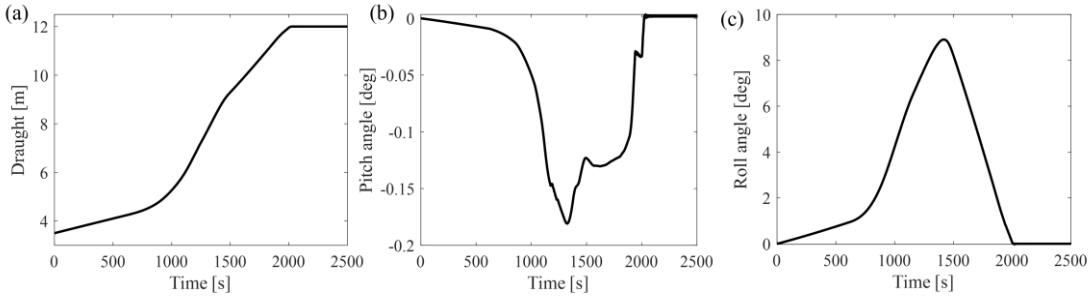

Figure 4.24. Draught, pitch, and roll angles during the ballasting without the controller in Case 3.

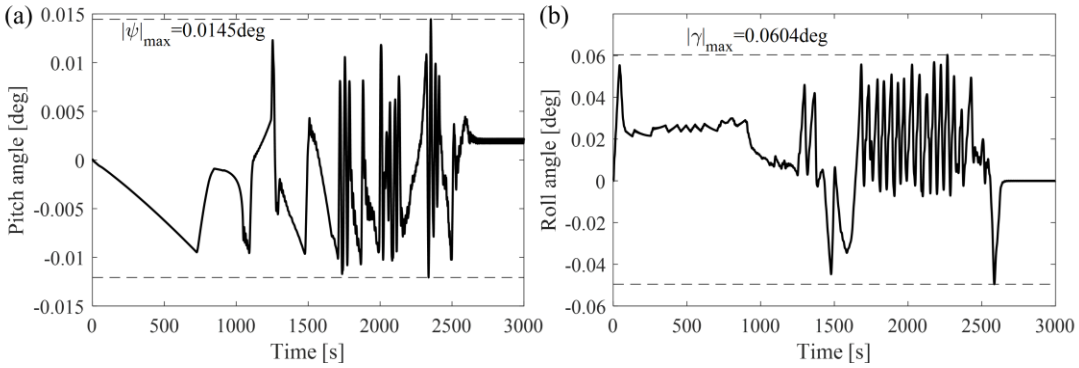

Figure 4.25. Pitch and roll angles during the ballasting with the modified P-controller in Case 4.

Summarized from the numerical results of Cases 1 - 4, the present modified P-controller can stabilize the pitch and roll angles during the ballasting and de-ballasting operations, and enhance the safety and efficiency of the dock.

4.4 Conclusions

The automatic ballast control of a floating dock is investigated using a numerical model capable of simulating the dynamic process of the dock during docking operations. The numerical model includes a 6-DOF model, a hydrostatic force model based on the Archimedes law using the strip theory, a hydrodynamic force model, and a hydraulic model for the hydraulic calculation of the ballast water system. To stabilize the dock, a modified P-controller is proposed based on the classical proportional controller, which controls the valve opening angle during the ballasting and de-ballasting operations.

The simulations reveal that without controllers, ballasting and de-ballasting operations result in roll angles larger than 8.9 deg and 13 deg, respectively, due to the asymmetric distribution of the ballast tanks. The modified P-controller is adopted to control the valves' opening angles and avoid large pitch and roll angles. The study investigates the effects of different control parameters on control performance and proposes a set of control inputs with good control performance. Reference control inputs can help keep the maximum pitch and roll angles not larger than 0.016 deg and 0.0783 deg, respectively. The study suggests that the present automatic control can be implemented in vessel docking simulations to improve the dock's stability during ballasting operations.

5. Dynamic Analysis of a Floating Dock under Accidental Conditions

5.1 Introduction

In this section, a comparison is made between the dynamic behavior of a floating dock (Model No.1) and a floating dock with a ship moored on top of it (Model No.2) is performed. Both models are shown in Figure 5.1. The geometry of the moored vessel is divided into sections, like the rest of the model. An example of a strip discretization is given in Figure 5.2. The number of sections of the vessel is independent of the number of sections of the dock since the hydrostatic forces are calculated for each body separately.

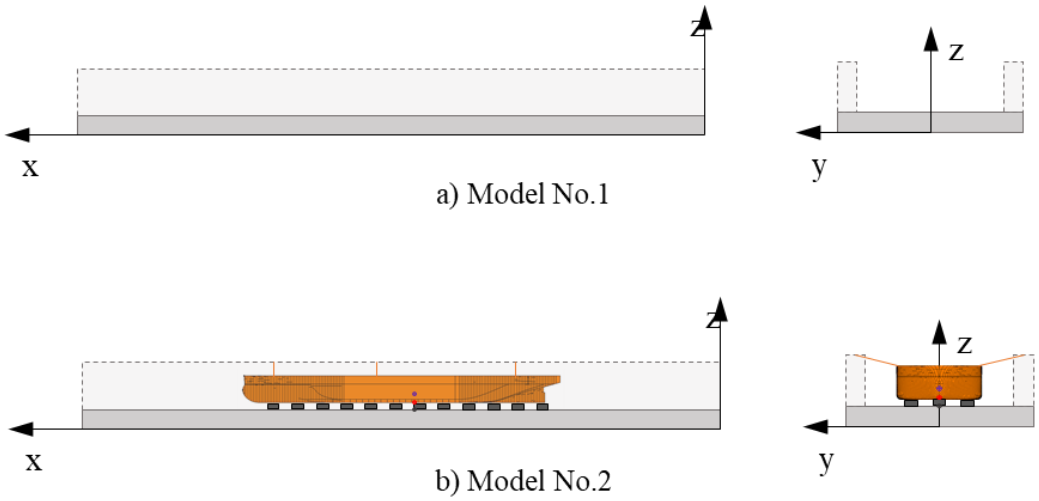

Figure 5.1. Illustration of a) the floating dock and b) the floating dock with a docked ship.

The modified P-controller developed is tested in a few simulations in which some of the components of the hydraulic model do not work as intended. These circumstances are called accidental conditions. The components of the hydraulic system selected are the valves giving access to the ballast tanks (ballast tanks' valves), and the hydraulic pumps used for de-ballasting, since in case of failure there is not a redundant element to replace them.

The differences between both model parameters are the dry mass, mass moments of inertia, and section of the rigid body, shown in Table 5.1. The center of gravity (CoG) is in a global Cartesian coordinate system with its origin in the stern of the dock, in the middle part of the breadth. In Model No.2, the CoG of the dock and the ship are aligned vertically, and as a result, the joint body has a higher CoG than the dock alone.

The objectives are to measure the dock's response, compare the dynamic behavior of the proposed models, anticipate possible accidents, and determine the critical components in the ballast water system of the floating dock.

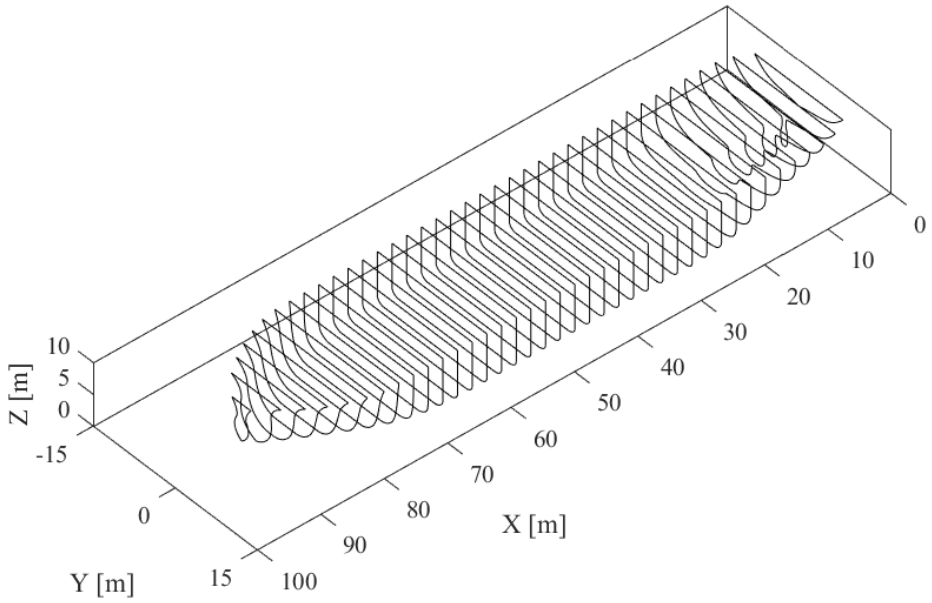

Figure 5.2. Strip discretization of the ship geometry. The number of sections is 40.

Table 5.1. Specification differences between models.

	x CoG (m)	y CoG (m)	z CoG (m)	I_{xx} (kgm^2)	I_{yy} (kgm^2)	I_{zz} (kgm^2)	Mass (ton)
Model 1	83.81	0.09	5.50	9.56×10^{8}	1.03×10^{10}	1.10×10^{10}	4637
Model 2	84.03	0.04	9.48	$1.32\text{x}10^{9}$	1.34×10^{10}	1.39×10^{10}	9766

5.2 Variable Independence Analysis

The sensitivity study of section number and point number of a section for the dock and the ballast tanks and the convergence study of the water level in ballast tanks are given by Zhang et al. [13]. Based on the convergent results of the section number and point number for the dock and the ballast tanks, the dock is discretized into 150 sections and each ballast tank is sliced into 20 sections in the present study. The number of points for a dock's section is 18 and those of port, center, and starboard tanks are 8, 8, and 6, respectively.

5.2.1 Mesh sensitivity analysis of the ship

The vessel's geometry is symmetrical between port and starboard but is non-symmetric between bow and stern. To estimate how many sections of the vessel and how many points in each section are needed to discretize the vessel according to the strip theory, two independent evaluations have been conducted. A sensitivity study of the section number and point number of a section is shown in Figures 5.4 and 5.5, where the displacement and x-coordinate of the center of buoyancy (CoB) for a vessel are depicted. A total of 50, 100, and 200 sections, and 102, 202, and 402 points per section are adopted for comparisons. The displacement and x-coordinate of CoB for each case exhibit good agreement with one another. The x-coordinate of CoB using 100 and 200 sections, in Figure 5.5 (b) match well with each other. Therefore, the results are convergent when using 100 sections to model the ship. For each section, 202 points are used to capture the complicated shapes of the vessel's sections at the stern.

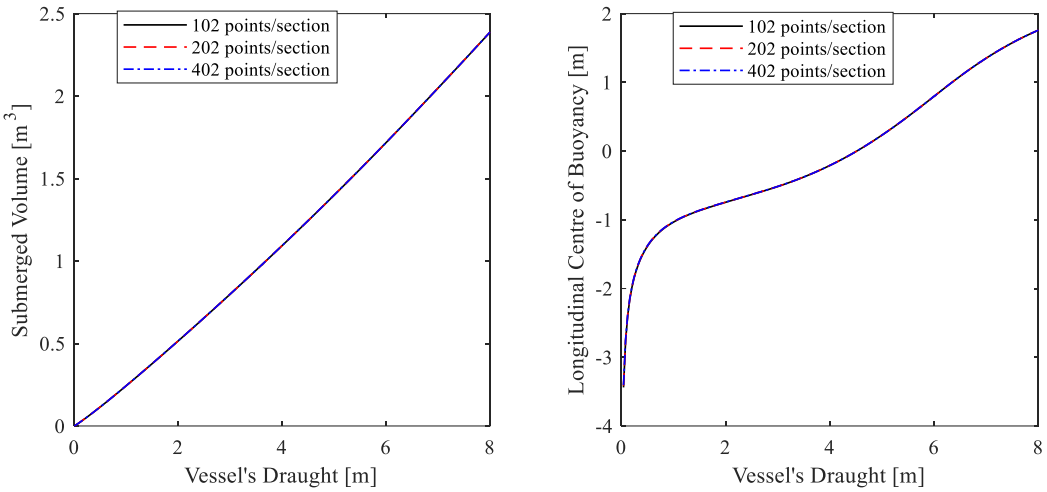

Figure 5.3. Sensitivity analysis for the number of points in each section for the vessel model. The total submerged volume of the vessel at a given draught (left). Location of the longitudinal center of buoyancy of the vessel at a given draught (right).

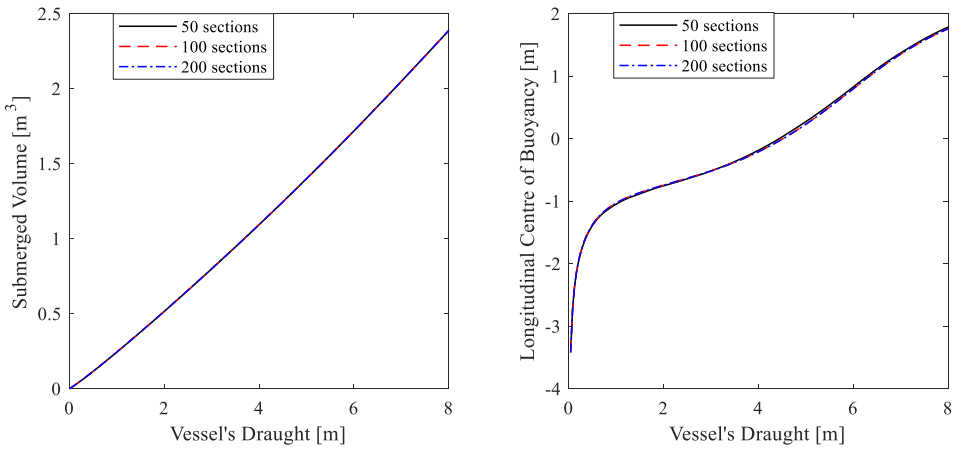

Figure 5.4. Sensitivity analysis for the number of sections used in the strip theory calculations for the vessel model. The total submerged volume of the vessel at a given draught (left). Location of the longitudinal center of buoyancy of the vessel at a given draught (right).

5.2.2 Time-step sensitivity study

The present numerical method and the proposed automatic ballast control had been successfully employed in Section 4. This section focuses on the analysis of the floating dock under accidental conditions. To ensure the accuracy of the model, a time-step sensitivity analysis is conducted. A series of simulations with three different time steps: Δt = 1 s, 0.5 s, and 0.25 s are performed. The purpose of these simulations is to evaluate the convergence of the results and verify the reliability of the computational model. Figure 5.3 presents the obtained results, showcasing the convergence and consistency achieved through the different time steps.

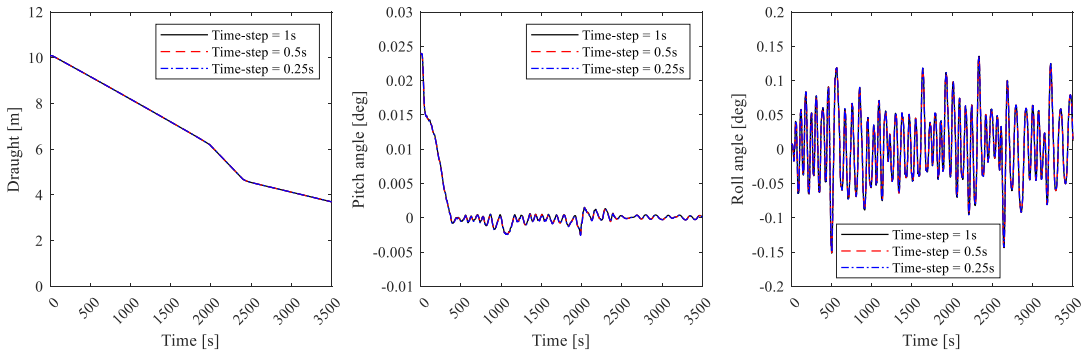

Figure 5.5. Time-step independence analysis.

Considering the need to optimize computational time while ensuring reasonably accurate results, a careful selection of the time-step becomes crucial. Thus, after thorough evaluation, a time-step of 1 s is considered appropriate for the subsequent analyses, which achieve a balance between computational efficiency and maintaining an acceptable level of precision in the predicted outcomes.

5.3 Model Evaluation

Given the disparities between the models, their dynamic responses are significantly influenced by factors such as system mass, damping, stiffness, and external forces. Consequently, the behaviors of the two models are distinct and not identical. In order to evaluate and compare the behavior of both models, a thorough analysis is conducted under various scenarios where the dock operates under normal conditions. The initial focus of the comparison is on the time history response during the de-ballast operation. The responses of the models are carefully examined, highlighting and analyzing the differences that arise. This analysis provides valuable insights into how each model behaves and performs during the de-ballast operation. Subsequently, a similar analysis is carried out during the ballast operation. The time history responses of both models are scrutinized and compared, enabling a comprehensive understanding of the disparities in their behaviors. By conducting these comparative analyses, we can gain valuable insights into the dynamic characteristics and performance differences between the two models. This investigation facilitates a deeper understanding of the system's behavior under regular operating conditions, shedding light on the nuanced variations between the models during de-ballast and ballast operations.

5.3.1 Model comparison during de-ballast operation

Two simulations of the de-ballasting operation under normal circumstances for both models are carried out. The initial draught of Model No.2 is set at 10.1 m when the vessel fully contacts the dock. In Model No.1, the ballast tanks are at maximum capacity at the starting point, yielding a draught of 11.5 m. A comparison of the time history of the draught, pitch angle, and roll angle of both models is shown in Figure 5.6.

The vertical velocity in the Model No.2 is smaller than in Model No.1, making the total operation time longer. At the same time, the controller can keep lower pitch angles in Model No.2 than in Model No.1. The reason is the increase in the necessary ballast water that needs to be evacuated to achieve the same draught due to the added weight of the vessel. This difference can be seen in Figure 5.8, where the percentage of water inside each tank after the operational draught is reached. The operational draught of the dock is 3.5 m. When the

floating dock stands in this position, the keel of the vessel on the dock's pontoon is completely above the water surface, and the inspection, maintenance, and repair can be performed accordingly. For this reason, all the de-ballasting operations stop at this draught, if possible.

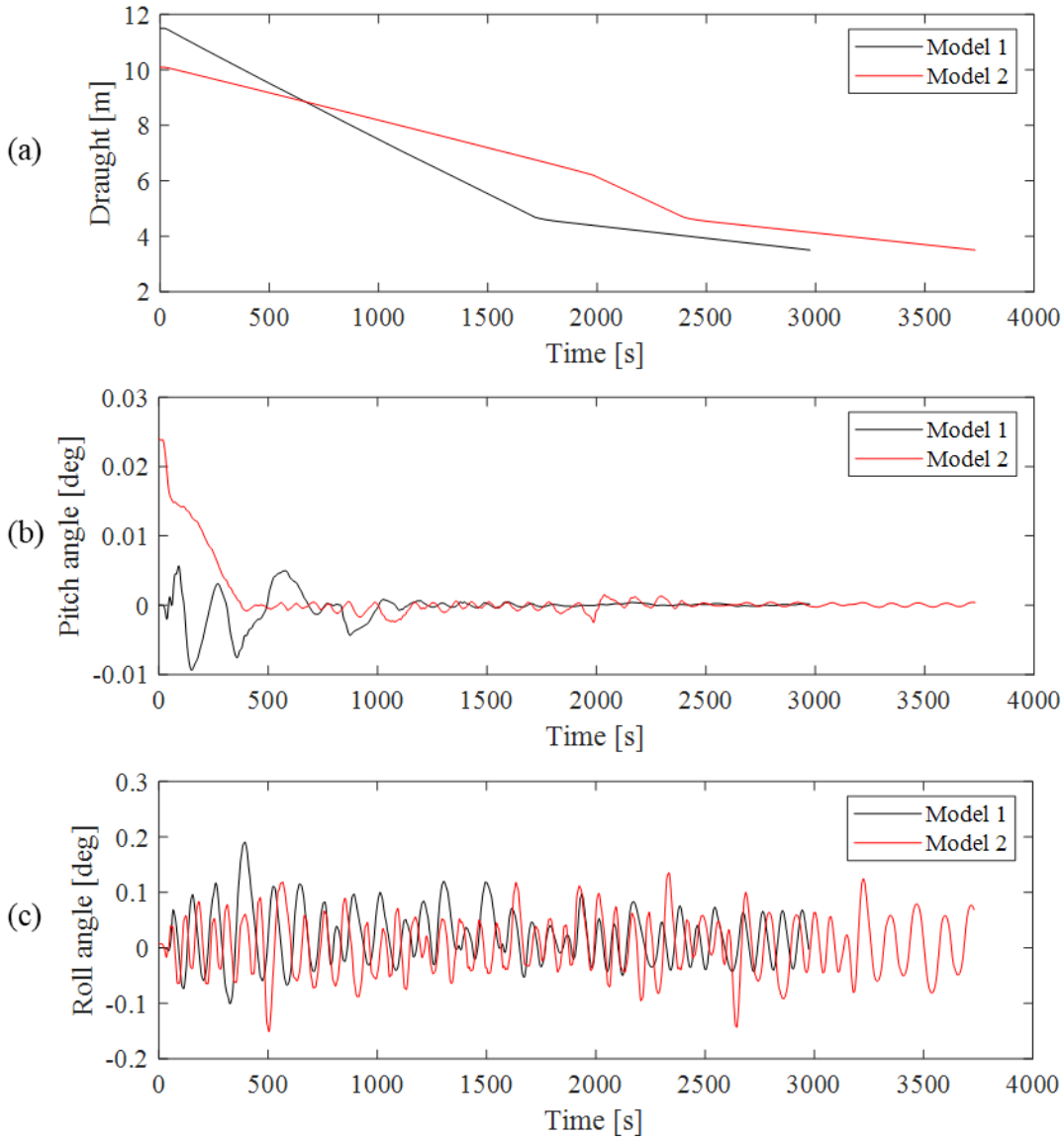

Figure 5.6. Motion response comparison between Models No.1 and No.2.

1	2	3	4	5	6
7	8	9	10	11	12
13	14	15	16	17	18

Figure 5.7. Ballast tank numbering configuration.

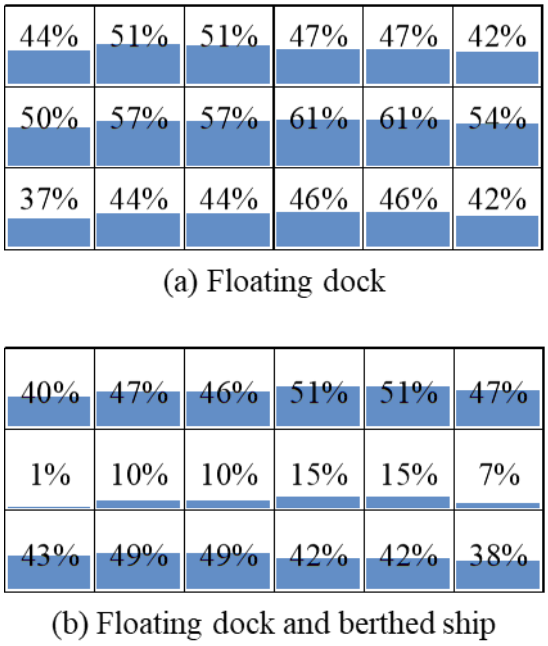

Figure 5.8. Ballast water volume percentage in each tank after de-ballasting for the floating dock (a), and for the floating dock with the docked ship (b). The final draught in both configurations is 3.5m.

5.3.2 Model comparison during ballast operation

The ballast operation starts at a draught of 3.5 m. The initial ballast water configuration is set to keep the heel and trim angles at 0 degrees when no external forces are applied. The operation is stopped when the dock reaches a draught of 10.1 m when the ship starts to have enough buoyancy to support itself.

In Figure 5.9, the time history of the draught, roll, and pitch motions is presented. The operational time is longer in Model No. 2 due to the increased amount of water needed to fill

the tanks, which have less volume of water to compensate for the mass of the ship. The final ballast water volume fraction in each tank is shown in Figure 5.10, for a draught of 10.1. The controller can keep the angular motions below the tolerance parameters.

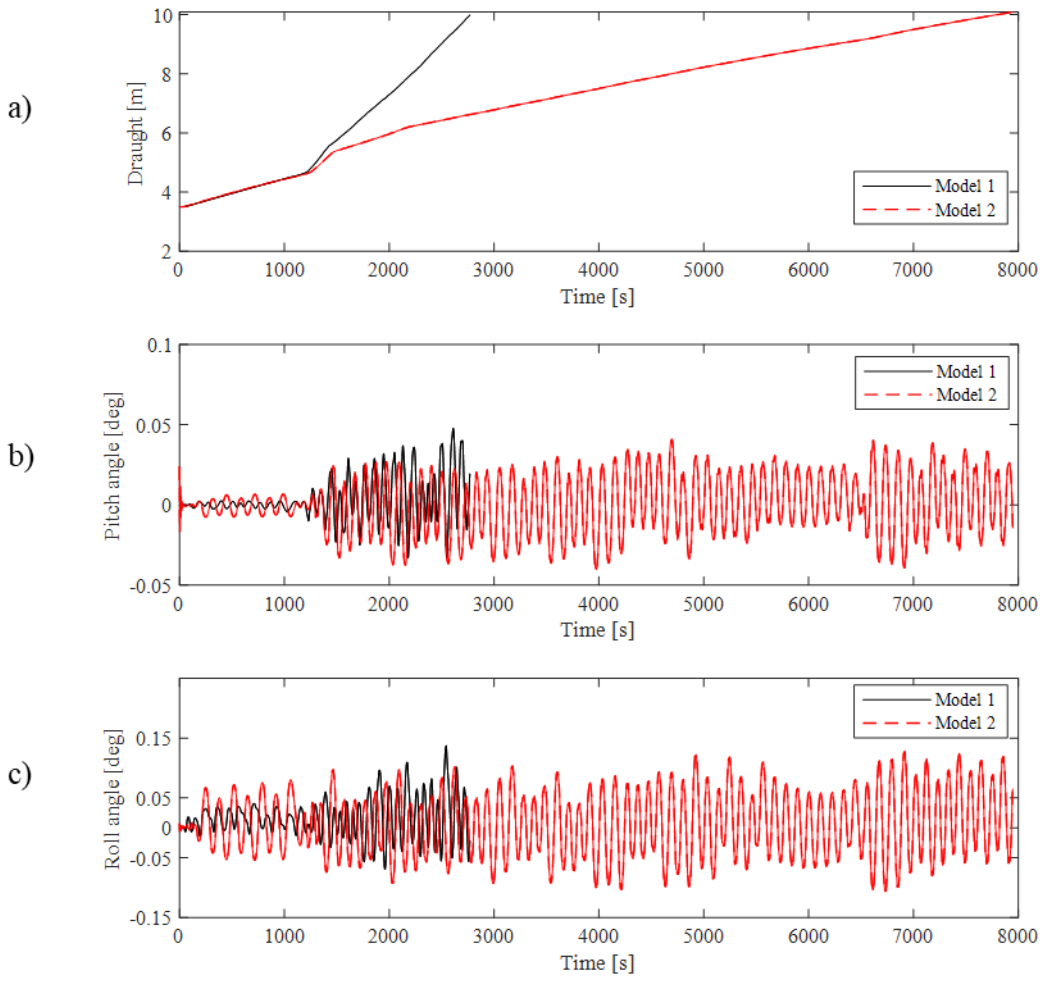

Figure 5.9. Motion response comparison between the ballasting operation for Model No.1 and Model No.2.

90%	91%	91%	85%	85%	90%
98%	98%	98%	98%	98%	98%
79%	79%	79%	86%	86%	91%

(a) Floating dock

92%	93%	94%	86%	86%	92%
98%	98%	98%	98%	98%	98%
82%	80%	80%	88%	88%	93%

(b) Floating dock and berthed ship

Figure 5.10. Ballast water volume percentage in each tank after ballasting for Model 1 (a), and Model 2 (b). The final draught in both configurations is 10.1 m.

5.3 Accident Scenarios for a Floating Dock

Many accidents in floating docks are related to the ballast water system, as seen previously. In this work, some accidental cases have been simulated where the components of the water ballast system fail during operation. Using the modified P-controller, the dock carries out its operation, reaching the target draught while maintaining the pitch and roll angles of the dock, and the docked vessel, at minimum values.

The simulations focus on the components that are prone to failure in the ballast water system, such as the valves in each ballast tank, de-ballasting pumps, and outlet valves in each of the six ballast water circuits. The most frequent failures of these components that could cause accidents in floating docks are highlighted. By identifying the potential sources of failure, the study aims to improve the safety of the ballast water system and prevent accidents from occurring.

In the different case scenarios, the maximum pitch and roll during the de-ballasting operation are compared to observe if the controller can perform the ballasting or de-ballasting of the dock in safe conditions. A limit angle is set by defining the maximum allowable draught difference between the port and starboard, and fore and aft. The limits are shown in Table 5.2.

Table 5.2. Maximum allowable angles

Movement	Maximum Draught (m)	Limit Angle (º)
Roll	0.4	0.574
Pitch	0.4	0.136

The model with the modified P-controller has been tested successfully before under normal operating conditions in Section 4. However, one of the strengths of the model is the capacity to simulate damaged conditions to predict the behavior of the dock and assess if the operation can be safely completed, or if it is possible to reduce the damage in case of an accident. Thus, some case scenarios are modeled here where a part of the dock's ballast water system fails.

5.3.1 De-ballasting operation cases for the floating dock model

(I) Ballast tanks' valve failure at different angles

It is assumed that the actuator of one of the ballast tank's valves is not working correctly, not being able to open the valve above different set angles. The maximum roll and pitch angles obtained during the ballasting operation of the floating dock are observed in Figure 5.11. In all the simulations the target draught of 3.5 m is reached.

It is observed that the controller can finish the operation successfully, keeping the stability of the dock at all times, even when there is a tank at maximum water volume fraction.

The differences observed when the opening angles are higher than 30º are negligible, however, when the angles are close to zero the motions are affected. In Figure 5.12, the time histories of the motion response of the two cases with the largest motions with valves No. 7 and 17 with an opening angle of 0º for Model No.1 are shown.

Opening angle	BT1	BT2	BT3	BT4	BT5	BT6	BT7	BT8	BT9	BT10	BT11	BT12	BT13	BT14	BT15	BT16	BT17	BT18
60º	0.15	0.15	0.18	0.12	0.12	0.14	0.13	0.13	0.13	0.22	0.22	0.22	0.18	0.19	0.15	0.19	0.18	0.15
45º	0.14	0.13	0.17	0.12	0.12	0.13	0.17	0.14	0.14	0.17	0.18	0.14	0.18	0.21	0.11	0.25	0.16	0.12
30º	0.13	0.15	0.16	0.15	0.15	0.13	0.14	0.15	0.15	0.17	0.16	0.21	0.23	0.20	0.16	0.20	0.26	0.17
15º	0.15	0.13	0.14	0.15	0.14	0.12	0.18	0.18	0.14	0.17	0.15	0.16	0.15	0.19	0.17	0.19	0.27	0.20
0º	0.15	0.13	0.14	0.15	0.14	0.12	0.18	0.18	0.14	0.17	0.15	0.16	0.16	0.19	0.17	0.19	0.27	0.20

(a) Maximum roll angle

Opening angle	BT1	BT2	BT3	BT4	BT5	BT6	BT7	BT8	BT9	BT10	BT11	BT12	BT13	BT14	BT15	BT16	BT17	BT18
60º	0.01	0.01	0.01	0.01	0.01	0.01	0.01	0.01	0.01	0.01	0.01	0.01	0.01	0.01	0.01	0.01	0.01	0.01
45º	0.01	0.01	0.01	0.01	0.01	0.01	0.01	0.01	0.01	0.01	0.01	0.01	0.01	0.01	0.01	0.01	0.01	0.01
30º	0.01	0.01	0.01	0.01	0.01	0.01	0.01	0.01	0.01	0.01	0.01	0.01	0.02	0.01	0.01	0.01	0.01	0.01
15º	0.01	0.01	0.01	0.01	0.01	0.01	0.02	0.01	0.01	0.01	0.01	0.01	0.01	0.01	0.01	0.01	0.01	0.01
0º	0.01	0.01	0.01	0.01	0.01	0.01	0.02	0.01	0.01	0.01	0.01	0.01	0.01	0.01	0.01	0.01	0.01	0.01

(b) Maximum pitch angle

Figure 5.11. Max. angular motions for Model No.1 when the opening angle of the ballast tank valve cannot open above the specified limit.

(II) Multiple ballast tanks' valve failure

Based on the numerical results in Section 5.3.1 (I), the present modified P-controller can stabilize the pitch and roll angles of the floating dock under one valve failure. To evaluate the reliability of the present modified P-controller of the floating dock, it is interesting to analyze the dock dynamic behavior with the different combinations of two valve failures. The maximum roll and pitch angles reached during the de-ballasting operation when two of the valves are closed are shown in Figure 5.13 and Figure 5.14 respectively.

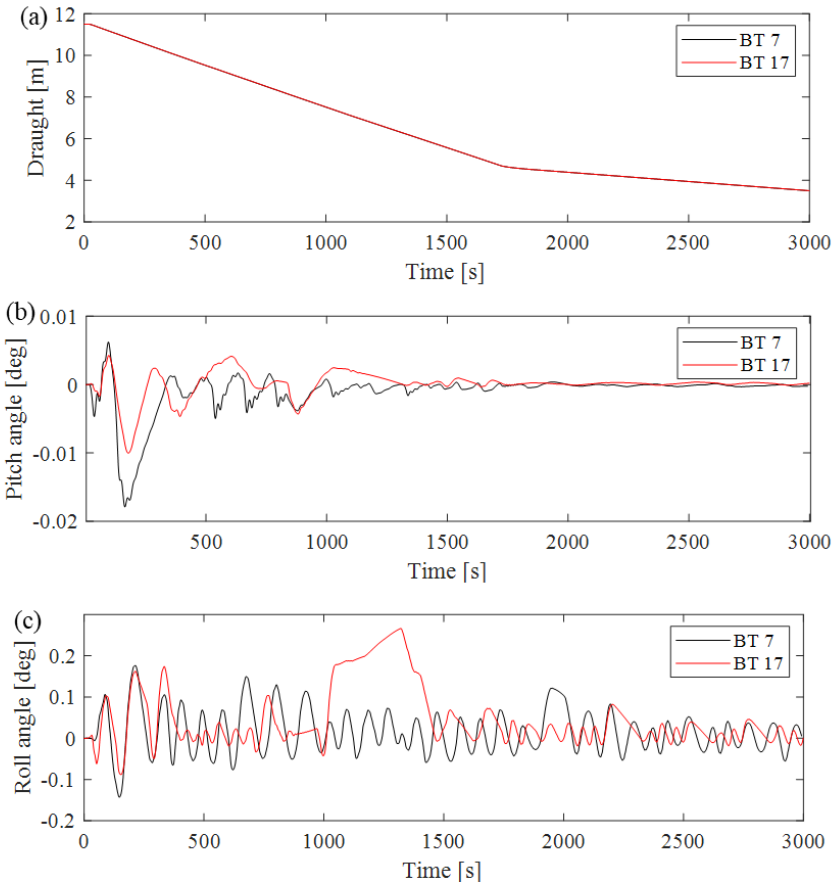

Figure 5.12. Motion response of the two cases with the largest motions with valves No. 7 and 17 with an opening angle of 0º for Model No.1.

1	0.15																	
2	0.14	0.13																
3	0.14	0.16	0.14															
4	0.93	0.61	0.18	0.15														
5	0.35	0.55	0.73	0.22	0.14													
6	0.59	0.72	0.95	0.15	0.14	0.12												
7	0.16	0.15	0.16	0.18	0.19	0.15	0.18											
8	0.14	0.15	0.12	0.16	0.19	0.14	0.13	0.18										
9	0.13	0.14	0.15	0.15	0.15	0.16	0.21	0.18	0.14									
10	0.15	0.21	0.21	0.16	0.17	0.12	0.19	0.17	0.22	0.17								
11	0.18	0.15	0.24	0.14	0.14	0.15	0.18	0.18	0.20	0.16	0.15							
12	0.18	0.24	0.20	0.13	0.14	0.16	0.16	0.13	0.15	0.19	0.20	0.16						
13	0.18	0.17	0.18	0.13	0.12	0.09	0.19	0.17	0.21	0.19	0.19	0.16	0.16					
14	0.18	0.14	0.19	0.13	0.15	0.18	0.15	0.22	0.23	0.17	0.19	0.21	0.94	0.19				
15	0.17	0.16	0.15	0.13	0.12	0.11	0.22	0.19	0.31	0.19	0.19	0.18	0.56	1.03	0.17			
16	0.15	0.16	0.12	0.12	0.14	0.16	0.23	0.22	0.18	0.20	0.17	0.17	1.38	1.11	1.21	0.19		
17	0.17	0.13	0.14	0.14	0.13	0.22	0.22	0.23	0.19	0.16	0.18	0.23	0.83	1.11	1.31	0.71	0.27	
18	0.13	0.13	0.14	0.12	0.14	0.14	0.21	0.18	0.18	0.20	0.20	0.18	0.97	0.92	1.44	0.53	0.45	0.20
Tank No.	1	2	3	4	5	6	7	8	9	10	11	12	13	14	15	16	17	18

Figure 5.13. Maximum roll angle (degrees) for Model No.1 during operation when 2 different ballast tank valves fail to open at the same time.

1	0.01																
2	0.02	0.01															
3	0.01	0.01	0.01														
4	0.01	0.01	0.01	0.01													
5	0.01	0.01	0.01	0.01	0.01												
6	0.01	0.01	0.01	0.01	0.01	0.01											
7	0.28	0.01	0.02	0.01	0.01	0.01	0.02										
8	0.01	0.11	0.02	0.01	0.01	0.01	0.01	0.01									
9	0.01	0.01	0.02	0.01	0.01	0.01	0.01	0.02	0.01								
10	0.01	0.01	0.01	0.02	0.01	0.01	0.02	0.01	0.01	0.01							
11	0.01	0.01	0.01	0.01	0.10	0.01	0.01	0.01	0.01	0.01	0.01						
12	0.01	0.01	0.01	0.01	0.01	0.27	0.01	0.01	0.01	0.01	0.01	0.01					
13	0.34	0.01	0.02	0.01	0.01	0.01	0.27	0.01	0.01	0.01	0.01	0.01	0.01				
14	0.01	0.17	0.01	0.01	0.01	0.01	0.01	0.10	0.01	0.01	0.01	0.01	0.03	0.01			
15	0.01	0.01	0.05	0.01	0.01	0.01	0.01	0.02	0.02	0.01	0.01	0.01	0.01	0.02	0.01		
16	0.01	0.01	0.01	0.05	0.01	0.01	0.01	0.01	0.01	0.02	0.01	0.01	0.01	0.01	0.01	0.01	
17	0.01	0.01	0.01	0.01	0.17	0.01	0.01	0.01	0.01	0.01	0.10	0.01	0.01	0.01	0.01	0.01	0.01
18	0.00	0.01	0.01	0.01	0.01	0.35	0.01	0.01	0.01	0.01	0.01	0.27	0.01	0.01	0.01	0.01	0.01	0.01
Tank No.	1	2	3	4	5	6	7	8	9	10	11	12	13	14	15	16	17	18

Figure 5.14. Maximum pitch angle (degrees) for Model No.1 during operation when 2 different ballast tank valves fail to open at the same time.

Larger roll angles occur when two ballast tanks on the same side of the dock cannot be de-ballasted, especially if one is in the bow and the other in the stern. Figure 5.15 shows the twelve most severe cases, with the colored ballast tanks representing where the valves fail. Note that those combinations generate roll angles higher than 200% of the discussed limit in Table 5.2.

In the pitch motion data, it is observed that angles of more than twice the predefined limit in Table 5.2 are also reached. These situations happen when the malfunctioning valves are both located in two tanks of the same ballast water circuit. In Figure 5.16, these cases are highlighted.

In general, it is observed that having two ballast tank valves failing at the same during the de-ballasting operation can induce high angular motions that can produce insecure situations in some cases. The modified P-controller is not able to keep the dock stable in these situations, and thus it is recommended to stop the operation in such cases.

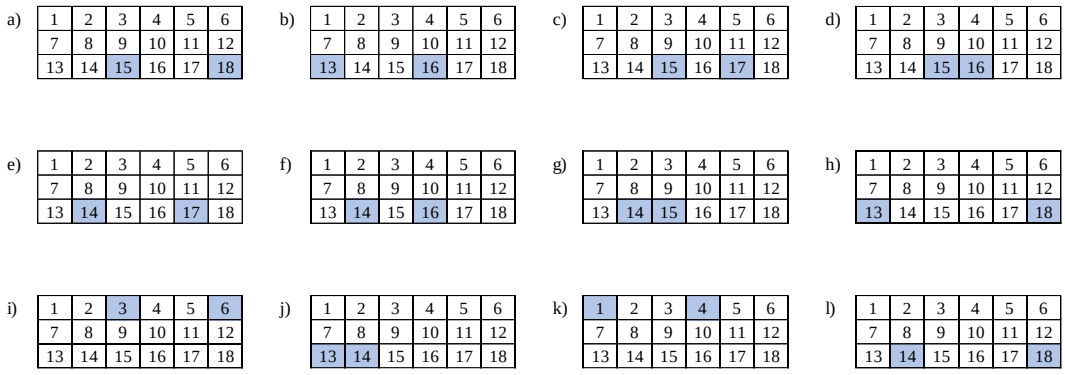

Figure 5.15. Ballast tank under failure configuration producing the highest roll angles. The twelve most severe cases.

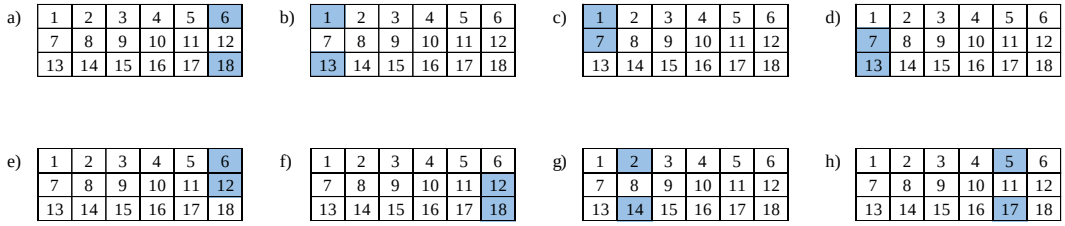

Figure 5.16. Combinations of closed ballast tanks' valves developing into excessive pitch angle situations.

(III) De-ballasting pump failure

The main function of the pumps is to pump the ballast water from the tanks out of the dock, to reduce the total weight of the dock, allowing the dock draught to decrease. Following previous arguments, different tests have been simulated where one or two of the de-ballasting pumps are turned off at the starting point. The maximum roll and pitch angles reached during the de-ballasting operation for the floating dock are shown in Figure 5.17. In all the tests, the desired draught has been reached.

For the cases of one pump failure, almost every configuration yields a successful operation, except when pumps No. 5 and 6 (responsible for ballast tanks No. 13, 14, 15, and 16, 17, 18) are not working, resulting in an excessive trim angle.

When two de-ballast pumps fail at the same time, the situations are more severe. If the two pumps not working are located in the stern of the dock, the roll motion will be excessive, while if the pumps are located near the fore section, the pitch angle would be too large.

1	0.261					
2	1.764	0.135				
3	1.773	1.840	0.191			
4	0.232	0.509	0.137	0.163		
5	1.265	1.035	0.159	0.180	0.186	
6	0.099	0.115	0.117	0.136	0.144	0.176
Tank No.	1	2	3	4	5	6

(a) Maximum roll angle

1	0.155					
2	0.705	0.054				
3	0.540	0.281	0.020			
4	0.355	0.094	0.013	0.173		
5	0.044	0.030	0.505	1.175	0.702	
6	0.007	0.807	1.507	2.073	2.541	1.518
Tank No.	1	2	3	4	5	6

(b) Maximum pitch angle

Figure 5.17. Maximum angles (degrees) obtained during operation when one or two of the de-ballasting pumps is off for Model No.1.

5.3.2 Gravitational ballasting operation cases for the floating dock model

(I) Ballast tanks' valves stuck at different angles

The gravitational ballasting is carried out without pumping. The controller adjusts the opening angle of the valves located on each ballast tank pipe to adjust the total water volume in each tank. If these valves do not open correctly, the tanks will not be filled up. The maximum roll and pitch angles obtained for each case in Figure 5.18 for different opening angles.

Opening angle	BT1	BT2	BT3	BT4	BT5	BT6	BT7	BT8	BT9	BT10	BT11	BT12	BT13	BT14	BT15	BT16	BT17	BT18
60°	0.12	0.11	0.10	0.12	0.11	0.10	0.16	0.17	0.13	0.12	0.13	0.11	0.15	0.16	0.09	0.16	0.16	0.18
45°	0.14	0.18	0.18	0.14	0.14	0.14	0.12	0.11	0.13	0.14	0.10	0.13	0.16	0.09	0.13	0.11	0.10	0.12
30°	0.12	0.24	0.25	0.30	0.15	0.12	0.12	0.18	0.12	0.11	0.17	0.17	0.13	0.14	0.76	0.67	0.11	0.14
15°	0.06	0.07	1.18	1.41	0.06	0.06	0.08	0.10	0.08	0.09	0.10	0.10	0.06	0.07	1.60	1.62	0.06	0.05
0°	0.13	0.19	1.52	1.63	0.14	0.14	0.13	0.14	0.16	0.17	0.10	0.13	0.14	0.13	1.61	1.64	0.15	0.13

(a) Maximum roll angle

Opening angle	BT1	BT2	BT3	BT4	BT5	BT6	BT7	BT8	BT9	BT10	BT11	BT12	BT13	BT14	BT15	BT16	BT17	BT18
60°	0.04	0.04	0.04	0.05	0.04	0.05	0.05	0.05	0.04	0.04	0.05	0.04	0.05	0.05	0.05	0.07	0.06	0.05
45°	0.14	0.05	0.04	0.04	0.05	0.11	0.05	0.03	0.04	0.04	0.04	0.04	0.06	0.06	0.05	0.04	0.05	0.09
30°	0.52	0.30	0.05	0.04	0.29	0.52	0.11	0.08	0.04	0.03	0.07	0.06	0.49	0.16	0.04	0.04	0.14	0.55
15°	1.03	0.39	0.02	0.02	0.36	0.98	0.10	0.04	0.04	0.03	0.04	0.09	1.50	0.50	0.03	0.04	0.51	1.50
0°	1.05	0.41	0.04	0.05	0.38	1.01	0.22	0.06	0.06	0.05	0.04	0.22	1.51	0.51	0.04	0.04	0.53	1.55

(b) Maximum pitch angle

Figure 5.18. Max. angles (degrees) during operation when different ballast tank valves cannot open above the opening angle for Model No.1.

The ballast operation is characterized by longer operational times since the water flow is lower than in the de-ballasting. In general, from the data, it is recovered that if the valves located in the middle of the port and starboard side (No. 3, 4, 15, 16) do not open properly, the roll angles are excessive, while if they are located in the corners of the dock (No. 1, 6, 13, 18), the pitch angle limit is exceeded. For some of these cases, the dock is not able to reach the target draught of 10.1. These cases can be seen in Figure 5.19.

A comparison of the time history of the draught, roll, and pitch motions is shown in Figure 5.20, where a regular operation is compared with a case in which one of the valves in the middle of the dock is closed (No. 9), and another in the extreme (No.18). The controller keeps the motion between tolerable limits, but sacrifices time when a valve is closed.

Opening angle	BT1	BT2	BT3	BT4	BT5	BT6	BT7	BT8	BT9	BT10	BT11	BT12	BT13	BT14	BT15	BT16	BT17	BT18
60º	10.1	10.1	10.1	10.1	10.1	10.1	10.1	10.1	10.1	10.1	10.1	10.1	10.1	10.1	10.1	10.1	10.1	10.1
45º	10.1	10.1	10.1	10.1	10.1	10.1	10.1	10.1	10.1	10.1	10.1	10.1	10.1	10.1	10.1	10.1	10.1	10.1
30º	10.1	10.1	10.1	10.1	10.1	10.1	10.1	10.1	10.1	10.1	10.1	10.1	10.1	10.1	10.1	10.1	10.1	10.1
15º	9.9	9.7	10.1	10.1	9.6	9.9	10.1	10.1	10.1	10.1	10.1	10.1	9.9	9.6	10.1	10.1	9.6	9.9
0º	9.9	9.7	10.1	10.1	9.7	9.9	10.1	10.1	10.1	10.1	9.7	10.1	9.9	9.7	10.1	10.1	9.7	10.0

Figure 5.19. Final draught (m) after the ballasting operation when different ballast tank valves cannot open above the opening angle for Model No.1.

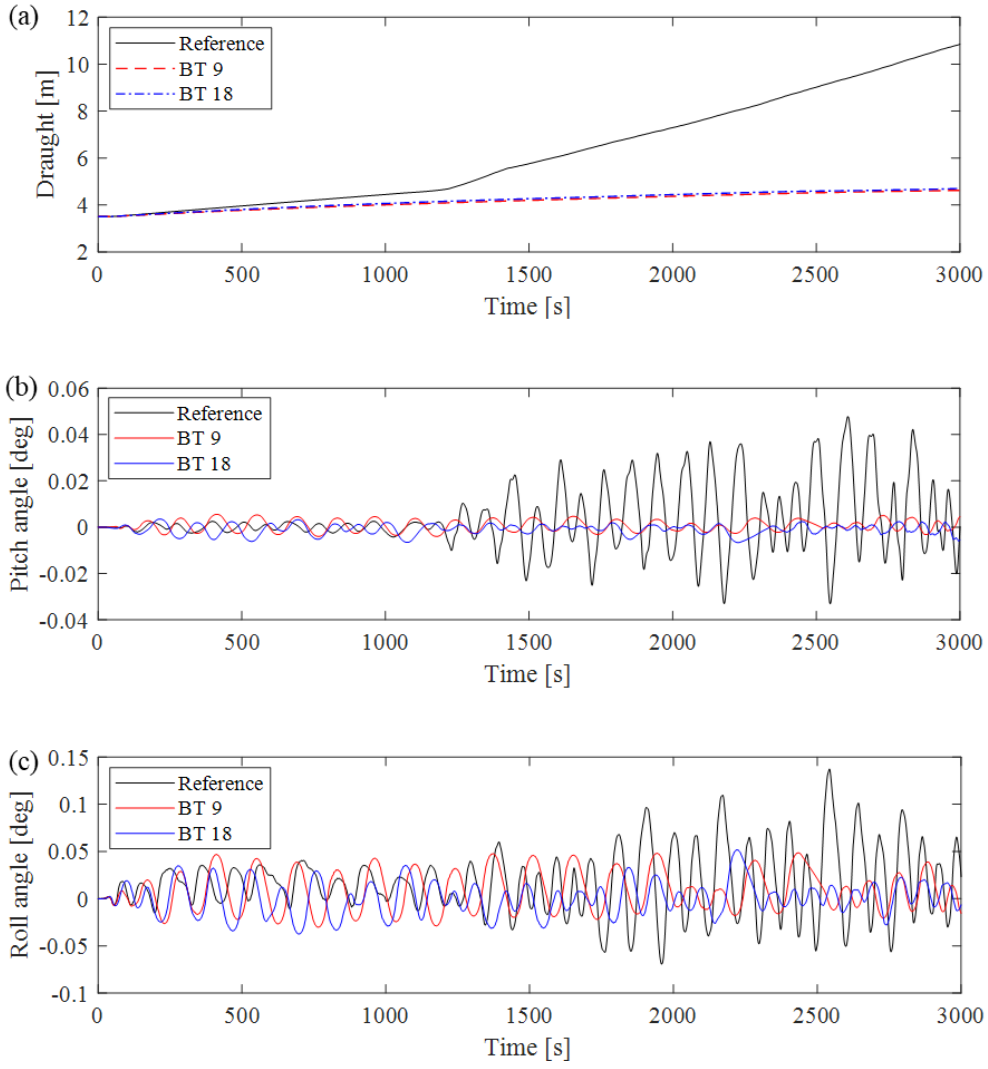

Figure 5.20. Graph comparing different ballasting procedures, comparing a normal situation to when different ballast tanks' valves are stuck at 15°. Draught (a), pitch (b), and roll (c) angle of the floating dock.

The operational time when a valve is closed is higher than in the regular operation and must be evaluated before continuing the operation. It is observed from these results that some valves are critical for the success of the operation. If any damage is observed on these valves, operations should be stopped immediately. Additionally, the maintenance program should include more tasks on these components than on the non-critical ones.

(II) Multiple ballast tanks' valves not opening

Based on the results in Section 5.3.2 (I), an operation could still be carried out if the damaged valve is not in the critical group. In this scenario, the probability of a second valve failing is not negligible. It is interesting to perform an analysis of different ballast operation scenarios where two valves of the ballast tanks fail to open. The maximum roll and pitch angle during these operations are shown in Figure 5.21 and Figure 5.22.

In general, it is observed that in most of the combinations, the stability of the dock is compromised, either for the roll or the pitch angle. Thus, it is not recommended to continue with operations when two ballast water tanks are not being filled during the ballasting operation.

1	0.13																	
2	4.68	0.19																
3	5.32	6.33	1.52															
4	6.39	7.78	8.97	1.63														
5	7.66	9.06	7.63	6.56	0.14													
6	8.26	7.71	6.30	5.58	4.89	0.14												
7	0.15	0.11	1.30	3.26	5.09	2.62	0.13											
8	0.13	1.32	2.48	4.46	4.96	2.21	0.13	0.14										
9	0.13	2.21	3.86	5.46	3.66	0.78	0.12	0.11	0.16									
10	0.76	3.63	5.30	3.98	2.32	0.13	0.13	0.12	0.13	0.17								
11	2.19	4.96	4.27	2.69	0.14	0.12	0.12	0.12	0.12	0.12	0.10							
12	2.64	5.06	3.04	1.73	0.14	0.13	0.09	0.14	0.10	0.12	0.12	0.13						
13	0.13	0.13	0.13	0.12	0.12	0.12	0.12	0.11	0.11	0.10	0.11	0.50	0.14					
14	0.11	0.11	0.11	0.10	0.39	0.08	0.11	0.10	0.10	0.13	1.49	2.40	0.10	0.13				
15	0.10	0.09	0.10	0.53	0.09	0.86	0.12	0.10	0.84	2.42	2.19	1.25	0.12	0.11	1.61			
16	0.08	0.07	0.28	0.10	0.10	0.09	1.25	2.11	2.52	0.50	0.12	0.11	0.12	4.83	6.26	1.64		
17	0.09	0.28	0.10	0.11	3.14	0.11	2.49	1.60	0.11	0.10	0.11	0.10	4.58	6.28	4.44	0.11	0.15	
18	0.16	0.10	0.11	0.13	2.04	0.12	0.20	0.11	0.11	0.10	0.12	0.12	4.95	4.23	0.11	0.12	0.11	0.13
Tank No.	1	2	3	4	5	6	7	8	9	10	11	12	13	14	15	16	17	18

Figure 5.21. Maximum roll angle (degrees) for Model No.1 during operation when 2 different ballast tank valves are closed at the same time.

1	1.05																	
2	0.06	0.41																
3	0.09	0.04	0.04															
4	0.04	0.07	0.04	0.05														
5	0.04	0.04	0.04	0.04	0.38													
6	0.03	0.04	0.04	0.05	0.04	1.01												
7	2.77	2.40	0.05	0.05	0.04	0.09	0.22											
8	2.18	0.03	0.05	0.04	0.05	0.08	2.48	0.06										
9	1.26	0.07	0.05	0.04	0.08	0.05	1.56	1.04	0.06									
10	0.08	0.04	0.04	0.04	0.04	1.56	0.58	0.23	0.04	0.05								
11	0.05	0.04	0.04	0.05	2.12	2.55	0.12	0.03	0.21	1.01	0.04							
12	0.06	0.04	0.04	0.05	2.76	3.79	0.03	0.10	0.62	1.56	3.66	0.22						
13	3.51	3.20	2.50	1.40	0.36	0.03	3.71	3.41	2.62	1.57	0.65	0.07	1.51					
14	3.52	3.34	2.50	0.98	0.02	0.48	3.50	3.16	1.85	0.60	0.04	0.03	3.13	0.51				
15	2.79	2.68	1.12	0.03	0.96	2.53	2.06	0.96	0.04	0.04	0.03	0.04	2.32	1.68	0.04			
16	1.49	0.98	0.03	1.47	2.97	2.95	0.04	0.04	0.03	0.05	1.28	2.64	0.64	0.07	0.03	0.04		
17	0.45	0.03	1.18	2.71	5.02	3.75	0.04	0.04	0.58	2.06	3.87	3.96	0.04	0.03	0.05	1.83	0.53	
18	0.03	0.42	1.53	2.65	4.34	3.93	0.08	0.71	1.66	2.74	3.75	3.80	0.03	0.04	0.75	2.34	4.00	1.55
Tank No.	1	2	3	4	5	6	7	8	9	10	11	12	13	14	15	16	17	18

Figure 5.22. Maximum pitch angle (degrees) for Model No.1 during operation when 2 different ballast tank valves are closed at the same time.

5.4 Accident Scenarios for a Floating Dock with a Docked Vessel

5.4.1 De-ballasting operation cases for the dock with a moored vessel

(I) Ballast tanks' valve failure at different angles

The total mass, mass moments of inertia, and geometry of Model No.2 are quite different from those of Model No.1, respectively due to the addition of the docked vessel. The maximum roll and pitch angles reached during the de-ballasting operation are shown in Figure 5.23 when one of the ballast tanks' valves is stuck at 0 degrees. The results show that the controller can keep its functionality, and the dock does not reach angles above the defined limit. There are no significant differences in comparison with Model No. 1.

Opening Angle	BT1	BT2	BT3	BT4	BT5	BT6	BT7	BT8	BT9	BT10	BT11	BT12	BT13	BT14	BT15	BT16	BT17	BT18
60°	0.13	0.14	0.14	0.14	0.12	0.15	0.15	0.16	0.16	0.16	0.15	0.15	0.16	0.15	0.15	0.16	0.17	0.16
45°	0.13	0.12	0.12	0.11	0.11	0.11	0.15	0.15	0.16	0.15	0.16	0.14	0.14	0.16	0.16	0.17	0.17	0.18
30°	0.11	0.12	0.11	0.11	0.10	0.11	0.16	0.17	0.16	0.15	0.16	0.18	0.18	0.17	0.16	0.16	0.17	0.17
15°	0.14	0.14	0.12	0.14	0.13	0.12	0.14	0.15	0.16	0.16	0.16	0.17	0.18	0.18	0.18	0.19	0.17	0.18
0°	0.14	0.14	0.12	0.14	0.13	0.12	0.14	0.15	0.16	0.16	0.16	0.17	0.18	0.18	0.18	0.19	0.17	0.18

(a) Maximum roll angle

Opening Angle	BT1	BT2	BT3	BT4	BT5	BT6	BT7	BT8	BT9	BT10	BT11	BT12	BT13	BT14	BT15	BT16	BT17	BT18
60°	0.02	0.02	0.02	0.02	0.02	0.02	0.02	0.02	0.02	0.02	0.02	0.02	0.02	0.02	0.02	0.02	0.02	0.02
45°	0.02	0.02	0.02	0.02	0.02	0.02	0.02	0.02	0.02	0.02	0.02	0.02	0.02	0.02	0.02	0.02	0.02	0.02
30°	0.02	0.02	0.02	0.02	0.02	0.02	0.02	0.02	0.02	0.02	0.02	0.02	0.02	0.02	0.02	0.02	0.02	0.02
15°	0.09	0.02	0.02	0.02	0.03	0.07	0.03	0.02	0.02	0.02	0.02	0.02	0.11	0.03	0.02	0.02	0.03	0.05
0°	0.09	0.02	0.02	0.02	0.03	0.07	0.03	0.02	0.02	0.02	0.02	0.02	0.11	0.03	0.02	0.02	0.03	0.05

(b) Maximum pitch angle

Figure 5.23. Max. angular motions (degrees) during operation when different ballast tank valves cannot open above the opening angle for Model No.2.

(II) Multiple ballast tanks' valve failure

Figures 5.24 and 5.25 show maximum roll and pitch angles for Model No.2 during operation when two different ballast tank valves fail at the same time. Compared with the results shown in Figures 5.13 and 5.14 for Model No.1, most combinations yield a stable operation. There are some exemptions, where the maximum pitch angle exceeds safety limits considerably. In these cases, the dock does not reach its operational draught of 3.5 m. These exemptions take place when the two valves are connected to tanks in the same hydraulic circuit, either near the bow or stern sections. These cases are presented in Figure 5.26.

From these results, it is clear that these valves are critical, and their condition must be monitored closely, to avoid unplanned maintenance stops. The conclusions drawn for Models No. 1 and 2 are similar, with the maximum angles reached with Model No. 2 being significantly lower.

1	0.14																
2	0.15	0.14															
3	0.16	0.16	0.12														
4	0.17	0.16	0.19	0.14													
5	0.16	0.17	0.15	0.16	0.13												
6	0.18	0.16	0.16	0.15	0.14	0.12											
7	0.13	0.17	0.16	0.15	0.14	0.16	0.14										
8	0.15	0.16	0.15	0.15	0.11	0.14	0.15	0.15									
9	0.16	0.15	0.16	0.13	0.12	0.13	0.16	0.15	0.16								
10	0.12	0.15	0.13	0.16	0.13	0.13	0.14	0.15	0.15	0.16							
11	0.15	0.14	0.13	0.13	0.13	0.15	0.17	0.14	0.16	0.18	0.16						
12	0.13	0.14	0.14	0.15	0.14	0.17	0.13	0.16	0.14	0.17	0.14	0.17					
13	0.13	0.14	0.13	0.13	0.12	0.12	0.19	0.18	0.19	0.18	0.18	0.18	0.18				
14	0.13	0.11	0.13	0.13	0.13	0.13	0.19	0.18	0.19	0.19	0.19	0.19	0.20	0.18			
15	0.12	0.13	0.13	0.12	0.13	0.12	0.20	0.20	0.21	0.18	0.19	0.19	0.19	0.15	0.18		
16	0.12	0.13	0.13	0.12	0.14	0.13	0.17	0.20	0.18	0.17	0.18	0.20	0.20	0.20	0.19	0.19	
17	0.13	0.13	0.14	0.14	0.15	0.14	0.19	0.18	0.18	0.18	0.19	0.18	0.20	0.20	0.20	0.22	0.17
18	0.12	0.13	0.13	0.12	0.15	0.14	0.20	0.18	0.18	0.18	0.19	0.20	0.17	0.15	0.17	0.21	0.18	0.18
Tank No.	1	2	3	4	5	6	7	8	9	10	11	12	13	14	15	16	17	18

Figure 5.24. Maximum roll angle (degrees) for Model No.2 during operation when 2 different ballast tank valves fail at the same time.

1	0.09																	
2	0.06	0.02																
3	0.09	0.11	0.02															
4	0.09	0.03	0.02	0.02														
5	0.02	0.02	0.03	0.05	0.03													
6	0.02	0.02	0.08	0.09	0.03	0.07												
7	0.99	0.07	0.05	0.03	0.03	0.03	0.03											
8	0.09	0.55	0.02	0.02	0.02	0.02	0.12	0.02										
9	0.09	0.02	0.03	0.02	0.02	0.08	0.03	0.02	0.02									
10	0.09	0.03	0.02	0.05	0.02	0.09	0.02	0.02	0.02	0.02								
11	0.03	0.02	0.02	0.02	0.51	0.09	0.02	0.02	0.02	0.02	0.02							
12	0.02	0.02	0.02	0.06	0.07	0.95	0.02	0.03	0.02	0.03	0.05	0.02						
13	0.44	0.06	0.04	0.05	0.03	0.02	1.15	0.07	0.09	0.09	0.03	0.03	0.11					
14	0.05	0.15	0.02	0.02	0.02	0.02	0.08	0.66	0.03	0.02	0.02	0.02	0.06	0.03				
15	0.05	0.02	0.04	0.02	0.02	0.04	0.07	0.02	0.09	0.02	0.02	0.02	0.04	0.12	0.02			
16	0.03	0.02	0.02	0.06	0.02	0.03	0.02	0.02	0.02	0.07	0.02	0.05	0.06	0.04	0.02	0.02		
17	0.02	0.02	0.02	0.02	0.18	0.03	0.02	0.02	0.02	0.03	0.59	0.08	0.02	0.02	0.04	0.06	0.03	
18	0.02	0.03	0.06	0.03	0.03	0.41	0.02	0.03	0.09	0.06	0.05	1.10	0.02	0.02	0.07	0.09	0.07	0.05
Tank No.	1	2	3	4	5	6	7	8	9	10	11	12	13	14	15	16	17	18

Figure 5.25. Maximum pitch angle (degrees) for Model No.2 during operation when 2 different ballast tank valves fail at the same time.

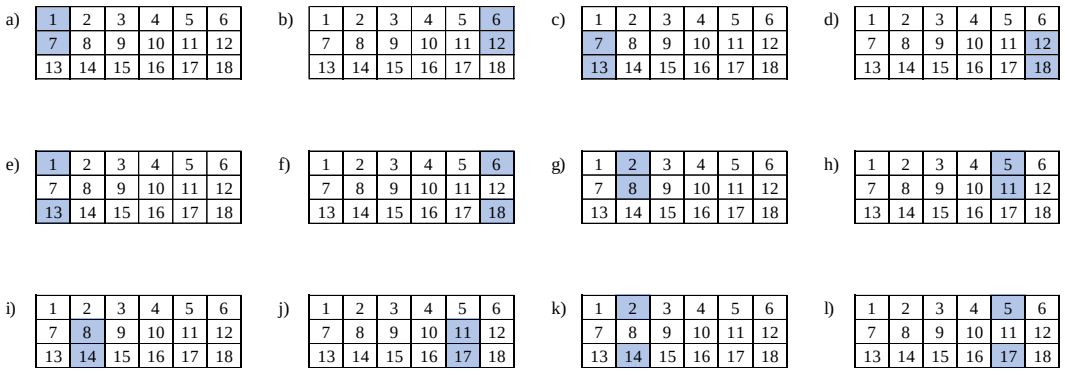

Figure 5.26. Ballast tank' valve failure combinations causing dangerous situations for Model No.2.

(III) De-ballast pump failure

As with Model No.1, the results from the simulations where one or two de-ballast pumps are failing during the operation are displayed in Figure 5.. When one de-ballast pump is turned off, it is observed again that the influence in the pitch motion is more relevant than for roll. The position of the pump turned off influences the maximum pitch angle reached, the cases where the pump is located on the stern are the most extreme.

1	0.139					
2	0.114	0.157				
3	0.168	0.134	0.116			
4	0.132	0.131	0.113	0.153		
5	0.129	0.123	0.118	0.160	0.111	
6	0.108	0.116	0.107	0.045	0.039	0.156
Tank No.	1	2	3	4	5	6

(a) Maximum roll angle

1	0.275					
2	0.552	0.128				
3	0.349	0.203	0.024			
4	0.072	0.033	0.024	0.085		
5	0.030	0.026	0.226	1.031	0.692	
6	0.231	1.233	2.053	2.607	3.115	2.127
Tank No.	1	2	3	4	5	6

(b) Maximum pitch angle

Figure 5.27. Maximum angles (degrees) obtained during operation when one or two of the de-ballasting pumps is off for Model No.2.

In the cases with two stopped pumps, on average the maximum angles are lower than for the Model No.1 cases. Only when the pumps located in the stern of the dock (No. 4-6) are turned off the trimming of the dock become excessive. Thus, it can be established that pumps No. 4, 5, and 6 are critical.

An interesting conclusion for these experiments lies in the leading diagonal of Figure 5.27. The maximum angular motions are reduced to tolerable values when two pumps in opposite directions are off. This statement opens the possibility to apply counteracting measures when one of the pumps fails, by turning off the opposite one. A series of simulations are carried out in which pump No. 6 is turned off from the beginning, and then pump No. 1, in the opposite direction, is turned off after different time windows, simulating the strategy described. In Figure 5.28 the dock's draught, roll, and pitch angles in the simulation are shown, where pump No. 1 is turned off after 300 s, 600 s, and 900 s. While the strategy can reduce the maximum trim angles during the de-ballasting, to keep the dock under stable limits, the second pump must be stopped in the very first minutes.

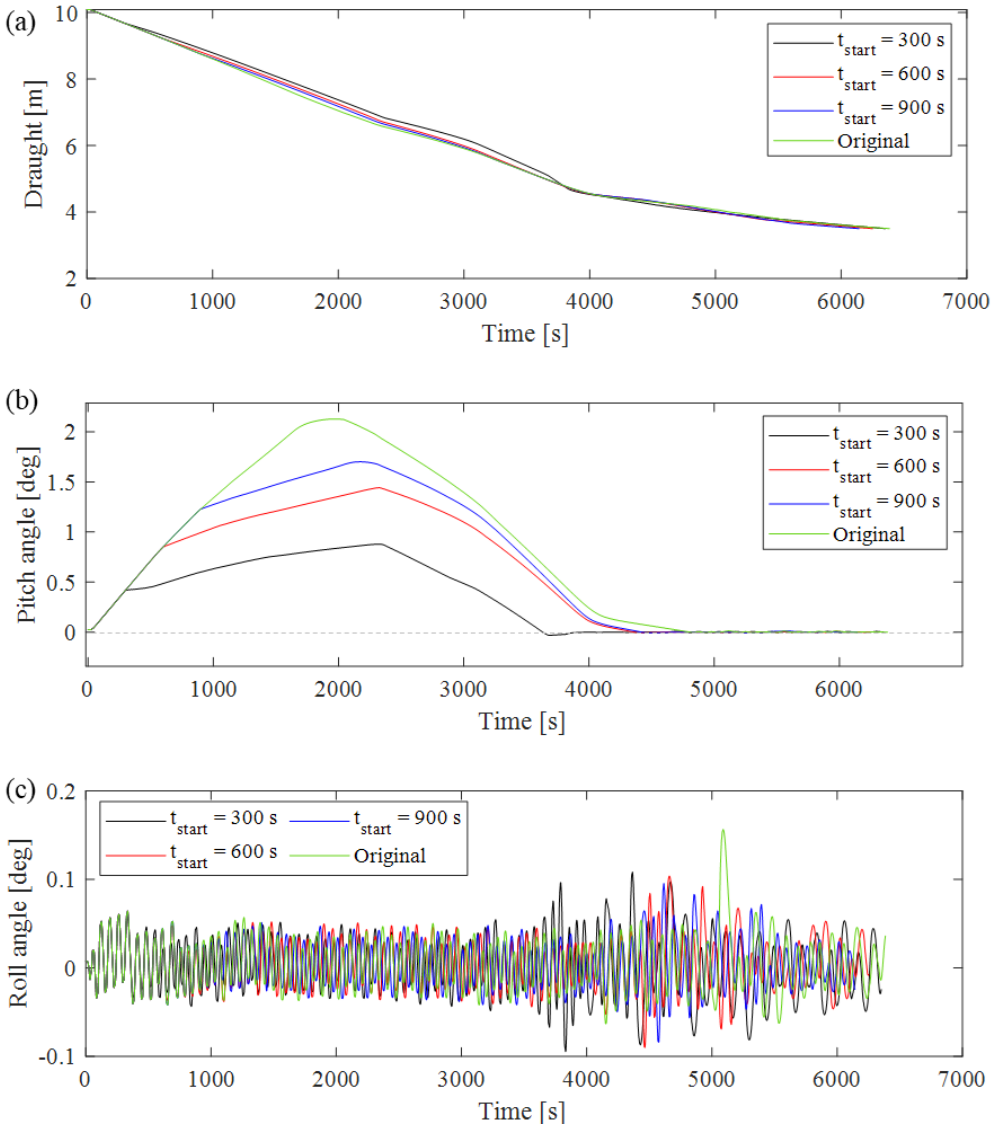

Figure 5.28. Time history motions of Model No.2 when, after finding pump No. 6 is disabled from the beginning, pump No. 1 is turned off after 300, 600, and 900 s.

5.4.2 Gravitational ballasting operation cases for the dock with a moored vessel

(I) Ballast tanks' valve failure at different angles

The maximum roll and pitch angles during the ballasting process are shown in Figure 5.29. When the valves are completely closed, the dock is not able to reach the target draught of 10.1 m. As a consequence, when all the ballast tanks are full, the weight distribution is not uniform, thus trimming and heeling the dock, because of the tank unable to be flooded.

Opening angle	BT1	BT2	BT3	BT4	BT5	BT6	BT7	BT8	BT9	BT10	BT11	BT12	BT13	BT14	BT15	BT16	BT17	BT18
60°	0.13	0.13	0.12	0.13	0.13	0.12	0.13	0.13	0.12	0.13	0.12	0.12	0.11	0.12	0.14	0.11	0.12	0.11
45°	0.13	0.13	0.12	0.13	0.13	0.12	0.13	0.13	0.12	0.13	0.12	0.12	0.11	0.12	0.14	0.11	0.12	0.11
30°	0.13	0.14	0.11	0.14	0.13	0.12	0.13	0.14	0.14	0.13	0.14	0.13	0.11	0.12	0.11	0.11	0.11	0.11
15°	0.13	0.14	0.12	0.12	0.12	0.12	0.11	0.12	0.13	0.13	0.12	0.11	0.10	0.11	0.11	0.32	0.12	0.10
0°	0.11	0.12	0.12	0.13	0.11	0.12	0.12	0.12	0.13	0.13	0.12	0.11	0.10	0.13	1.71	1.97	0.11	0.11

(a) Maximum roll angle

Opening angle	BT1	BT2	BT3	BT4	BT5	BT6	BT7	BT8	BT9	BT10	BT11	BT12	BT13	BT14	BT15	BT16	BT17	BT18
60°	0.05	0.04	0.04	0.04	0.05	0.04	0.05	0.04	0.05	0.04	0.04	0.04	0.04	0.04	0.05	0.04	0.04	0.04
45°	0.05	0.04	0.04	0.04	0.05	0.04	0.05	0.04	0.05	0.04	0.04	0.04	0.04	0.04	0.05	0.04	0.04	0.04
30°	0.04	0.04	0.04	0.04	0.04	0.04	0.04	0.05	0.04	0.05	0.05	0.04	0.05	0.04	0.04	0.04	0.04	0.04
15°	0.19	0.05	0.04	0.04	0.05	0.04	0.13	0.05	0.04	0.05	0.07	0.11	0.22	0.05	0.04	0.04	0.05	0.21
0°	1.02	0.37	0.04	0.04	0.05	0.05	0.16	0.05	0.04	0.05	0.38	0.82	1.39	0.46	0.04	0.04	0.35	1.33

(b) Maximum pitch angle

Figure 5.29. Maximum angles (degrees) during operation when different ballast tank valves cannot open above the opening angle for Model No.2.

(II) Multiple ballast tanks' valve failure

In this case, the dock is not able to reach its target draught of 10.1 m in any of the cases. The dock trimming and heeling is large due to the weight imbalance. In Figure 5.30, the final draught for all the cases is shown.

1	9.81																	
2	8.34	9.68																
3	8.53	8.66	9.77															
4	8.82	8.93	8.42	9.73														
5	9.08	9.19	8.29	8.21	9.31													
6	9.33	9.11	8.38	8.02	7.78	9.38												
7	9.25	9.11	8.75	9.02	9.08	9.28	9.81											
8	9.26	9.14	8.82	9.04	9.19	9.21	8.83	9.89										
9	9.33	9.17	9.19	9.18	9.09	9.12	9.15	9.33	10.04									
10	9.36	9.21	9.06	9.17	8.73	8.74	9.47	9.44	9.72	10.09								
11	9.38	9.38	9.00	8.80	8.60	8.40	9.52	9.76	9.59	9.83	10.09							
12	9.48	9.47	8.96	8.60	8.30	8.22	9.88	9.51	9.93	9.77	9.56	10.09						
13	9.40	9.26	8.42	8.91	9.12	9.47	8.27	8.44	9.44	9.45	9.44	9.62	9.83					
14	9.39	9.27	8.65	9.07	9.49	9.24	8.45	8.55	9.31	9.31	9.59	9.83	8.90	9.69				
15	9.48	9.39	9.10	9.37	9.27	9.08	8.76	8.99	9.32	9.70	9.60	9.42	8.81	8.64	9.94			
16	9.55	9.24	9.47	9.14	8.78	8.61	9.02	9.07	9.75	9.43	9.32	9.31	8.94	9.21	9.48	9.97		
17	9.60	9.42	9.14	8.67	8.35	8.19	9.36	9.09	9.31	9.31	9.25	9.26	9.40	9.49	9.21	8.64	9.70	
18	9.74	9.13	8.96	8.41	8.13	7.99	9.47	9.32	9.46	9.46	9.45	9.26	9.61	9.39	8.97	8.77	8.89	9.85
Tank No.	1	2	3	4	5	6	7	8	9	10	11	12	13	14	15	16	17	18

Figure 5.30. Final draught after ballasting of Model No.2 when 2 different ballast tank valves are closed.

5.4 Conclusion

A comprehensive analysis of the floating dock under different accidental conditions has been carried out. The dynamic behavior of the dock changes considerably when there is a docked vessel on the pontoon deck. It is necessary to conduct individual analyses in the different scenarios to assess the stability risks.

In case of a component of the hydraulic system not working as intended, the floating dock is capable of reaching the target draught during the de-ballasting process, with occasional excessive roll or pitch angles in some cases. Even when there is a docked vessel on deck, the controller maintains the motions of the dock in safe conditions. In the ballasting operation, the difference in having a vessel docked is more notable. The single dock can reach the target draught in almost every scenario, but when the additional mass of the ship is added, the corresponding target draught becomes unreachable.

6. Conclusions

In the present study, a dynamic analysis of the floating dock under accidental conditions is performed using a digital floating dock model that incorporates a 6-DOF model, a hydrostatic force model, a hydrodynamic force model, a hydraulic model, and a modified P-controller. The dynamic processes of the floating dock during the ballasting and de-ballasting operations with and without valve and pump failures are simulated, and the control performance of the present modified P -controller is evaluated in these failure cases. The main results of this study are summarized as follows:

(1) The simulations reveal that without controllers, ballasting and de-ballasting operations result in roll angles larger than 8.9 deg and 13 deg, respectively, due to the asymmetric distribution of the ballast tanks. The modified P-controller is adopted to control the valves' opening angles and avoid large pitch and roll angles, and its control parameters are optimized. Reference control inputs can help keep the maximum pitch and roll angles not larger than 0.016 deg and 0.0783 deg, respectively. The study suggests that the present automatic control can be implemented in vessel docking simulations to improve the dock's stability during ballasting operations.

(2) In cases of valve or pump failure, the present modified P-controller exhibits excellent performance in de-ballasting operation cases with tank valve failure, while it is easy to fail for most of the pump failure during the de-ballasting cases and the valve failures during the ballasting cases.

The results demonstrate that the controller is capable of generating ballast or de-ballast strategies that effectively minimize the heeling and trimming of the dock. This risk reduction significantly lowers the chances of accidents by appropriately opening or closing the various valves on the dock. As a result, a dock master can operate the floating dock using the numerical model, thereby reducing the required training periods.

.

References

[1] International Maritime Organization (IMO), 1974. International Convention for the Safety of Life at Sea (SOLAS), 1 November 1974, 1184 UNTS 3, available at: https://www.refworld.org/docid/46920bf32.html, accessed 26 January 2023.

[2] House, D. J., 2005. Chapter 1 in Dry Docking and Shipboard Maintenance.

[3] Wankhede, A., 2021, Dry Dock, Types of Dry Docks & Requirements for Dry Dock, last modified 9 January 2021. https://www.marineinsight.com/guidelines/dry-dock-types-of-dry-docks-requirements-for-dry-dock/#Types_of_Dry_Dock.

[4] Gudmestad, O. T., 2015, Marine Technology and Operations: Theory & Practice. WIT Press.

[5] Korotaev, V. V., Pantiushin, A. V., Serikova, M. G., & Anisimov, A. G. 2016. Deflection measuring system for floating dry docks. Ocean Engineering, 117, 39 – 44.

[6] Heger Dray Dock, INC, 2005. Dockmaster Training Manual.

[7] Rajewski, P., 2018. Impact of Dock Tanks Pumping Plan on Structural Loads of a Dock and a Ship. New Trends in Production Engineering, 1(1), 143-149.

[8] Ohkawa, T., Itoh, M., Matsunaga, H., Horiguchi, K., & Sato, K., 1984. Automatic ballast control for floating dock.

[9] Guo, T., Zhang, R., & Zhou, S. H. 2014. Design of automatic control system of floating dock. Applied Mechanics and Materials, 527, 237–241. https://doi.org/10.4028/www.scientific.net/AMM.527.237.

[10] Topalov, A., Kozlov, O., Gerasin, O., Kondratenko, G., & Kondratenko, Y., 2018. Stabilization and control of the floating dock's list and trim: Algorithmic solution. Proceedings of the 14th International Conference on Advanced Trends in Radioelectronics, Telecommunications and Computer Engineering, 1217–1222.

[11] Kusuma, I. R., 2017. Design and Simulation of Automatic Ballast System on Catamaran Ship Based on Programmable Logic Control. International Journal of Marine Engineering Innovation and Research, 1(3), 161–167.

[12] Bara, C., Cornoiu, M., & Popescu, D., 2012, An optimal control strategy of ballast systems used in ship stabilization. Proceedings of the 20th Mediterranean Conference on Control and Automation, 878–883.

[13] Zhang, J., Wen, X., and Ong, M. C., 2023. Development of a floating dock numerical model and the ballast water distribution strategy, Proceedings of the 42nd International Conference on Offshore Mechanics and Arctic Engineering (OMAE2023). American Society of Mechanical Engineers, Melbourne, Australia, June 11-16, 2023. (Submitted: OMAE2023-102996).

[14] Kaup, M., Łozowicka, D., & Blatnický, M., 2018. Selected problems of ship safety in the process of docking. New Trends in Production Engineering, 1(1), 43–49.

[15] National Transportation Safety Board, (2012), Dockside capsizing and sinking of towing vessel invader and Dry Dock #3. Marine Accident Brief.

[16] BUSINESS & FINANCE, 2015. Scandlines ferry damaged while undocking at Remontowa. https://www.offshore-energy.biz/scandlines-ferry-damaged-while-undocking-at-remontowa/

[17] Landowski, G., 2017. Dock with tanker tilts in NAUTA Shipyard, last modified 4 May 2017. https://www.polandatsea.com/dock-with-tanker-tilts-in-nauta-shipyard/

[18] Faltinsen, O. M., and Svensen, T., 1990. Incorporation of seakeeping theories in CAD, International Symposium on CFD and CAD in Ship Design, MARIN, Wageningen, Netherlands.

[19] Journée, J.M.J., Adegeest, L.J.M., 2003. Theoretical manual of strip theory program “SEAWAY for Windows”. Delft University of Technology.

[20] Bandyk, P. J., 2009. A body-exact strip theory approach to ship motion computations. University of Michigan.

[21] Faltinsen, O. M., 1993. Wave induced motions and loads on ships: Theory and numerical methods. Paper presented at UETP Course on New Techniques for Assessing and quantifying vessel stability and seakeeping qualities, March 1993. http://resolver.tudelft.nl/uuid:2e03ef83-d023-41aa-9ca7-d90450ef14c5

[22] Astrom, K. J., & Hagglund, T., 2010. Advanced PID control. Instrument Society of America.

[23] Franklin, G. F., Powell, J. D., Emami-Naeini, A., & Powell, J. D., 2002. Feedback control of dynamic systems (Vol. 4). Upper Saddle River: Prentice Hall.

[24] Ogata, K., 2010. Modern control engineering (Vol. 5). Upper Saddle River, NJ: Prentice Hall.

[25] Newman, J. N., 2018. Marine hydrodynamics, pp. 448. The MIT Press.

[26] Falkovich, G., 2011. Fluid mechanics: A short course for physicists. Cambridge University Press.

[27] Eurotorc, 2022. Butterfly valve engineering data, last modified November 12, 2022, https://www.eurotorc.com/butterfly-valve-engineering-data.html.

[28] Shaub, H., Junkins, J.L., 2009. Analytical Mechanics of Space Systems. American Institute of Aeronautics and Astronautics (AIAA)

[29] Zhang, J., Li, L., Ong, M. C., EI Beshbichi, O., and Kniat, A. “Development of a Response Assessment Tool for a Floating Dock System”. Proceedings of the 41st International Conference on Offshore Mechanics and Arctic Engineering (OMAE2022). American Society of Mechanical Engineers, Hamburg Germany, June 5–10, 2022. V05BT06A014.

[30] Pabst W., “Theory of the landing impact of seaplanes”, National Advisory Council for Aeronautics (NACA) Technical Memorandum No.580, Washington, USA (1930).

[31] Det Norske Veritas (DNV)., 2012. “DNV Recommended Practice DNV-RP-C205: Environmental conditions and environmental loads”.